

Constrained Probabilistic Movement Primitives for Robot Trajectory Adaptation

Felix Frank, Alexandros Paraschos, Patrick van der Smagt, Botond Cseke

Abstract—Versatile movement representations allow robots to learn new tasks and rapidly adapt them to environmental changes, e.g. introduction of obstacles, placing additional robots in the workspace, modification of the joint range due to faults or range of motion constraints due to tool manipulation. Probabilistic movement primitives (ProMP) model robot movements as a distribution over trajectories and they are an important tool due to their analytical tractability and ability to learn and generalise from a small number of demonstrations. Current approaches solve specific adaptation problems, e.g. obstacle avoidance, however, a generic probabilistic approach to adaptation has not yet been developed. In this paper we propose a generic probabilistic framework for adapting ProMPs. We formulate adaptation as a constrained optimisation problem where we minimise the Kullback-Leibler divergence between the adapted distribution and the distribution of the original primitive and we constrain the probability mass associated with undesired trajectories to be low. We derive several types of constraints that can be added depending on the task, such as joint limiting, various types of obstacle avoidance, via-points, and mutual avoidance, under a common framework. We demonstrate our approach on several adaptation problems on simulated planar robot arms and 7-DOF Franka-Emika robots in single and dual robot arm settings.

I. INTRODUCTION

LEARNING a robotic task from the ground up is a considerable effort: since action and sensor space are very high-dimensional, the number of repeats needed to get a reasonable representation of these spaces is typically too large, and execution on a real robot takes too long. A good way to improve the sample efficiency is to add prior knowledge, like a model of the environment or a feasible start solution, to the learning process. In this paper, we efficiently incorporate prior knowledge through demonstration, relying on humans to show possible solutions to a specific task to a robot, from which it can then generalise. There are various frameworks to learn from such demonstrations. These typically break down complex tasks into simple movements, called movement primitives, which can be learned from such demonstrations and subsequently combined in order to solve complex tasks.

We distinguish two approaches to movement primitives: (i) *deterministic* approaches, such as dynamic movement primitives (DMP) [1], [2], which learn a deterministic average of the given demonstrations; and (ii) *probabilistic* approaches, such as probabilistic movement primitives (ProMP) [3] or Gaussian mixture models with Gaussian mixture regression (GMM-GMR) [4], which, in addition, can learn the inherent

variability in the demonstrations. Dynamic movement primitives model robot trajectories with an attractor, determining the end point of a trajectory, and a learned forcing function, which shapes the path of the robot towards the attractor.

Probabilistic approaches rely on probability distributions to capture multiple given trajectories and their variance. Some methods directly model trajectories in the demonstrated space with Gaussian mixture models [4], whereas other methods learn the parameters of a mixture of linear Gaussian state-space models [5] to best represent the given trajectories. Probabilistic movement primitives (ProMPs) represent the distribution over trajectories by a linear combination of a stochastic weight vector and a set of basis functions [3].

In practice there is a wide variety of potential tasks and it is impractical to demonstrate every possible variation to the robot beforehand. Therefore a central element in every movement primitive framework is the ability to adapt primitives to unseen scenarios. Bayesian approaches model full posterior distributions instead of just yielding a point estimate. This gives additional freedom—for example, if only the endpoint of a trajectory is constrained, the flexibility on how to get there remains largely untouched. The remaining variability can then be exploited further downstream, for instance to satisfy further constraints or to optimise some criterion. Since deterministic solutions have no means to encode this additional tolerance, extending them with further requirements—a via point for example—is not possible in a natural way.

There is extensive literature on adapting the different primitive frameworks to specific tasks. The DMP formulation has been extended to include obstacle avoidance [6]–[9], as well as joint limits [10] and limits on the robot velocity [11]. In the probabilistic frameworks one direction of research combines multiple primitives together in one primitive [12]–[16], allowing adaptation by *including* additional behaviour into a primitive. Conversely, robotic problems like avoidance or respecting joint limits are typically easier to formulate by *excluding* specific behaviour from a primitive. In this direction, obstacle avoidance for ProMPs has been investigated in [17]–[19], nonetheless, a probabilistic approach tackling primitive adaptation in a generic way is missing so far.

In this paper we extend the ProMP framework with the ability to add constraints to a given primitive. Therefore, we formulate adaptation as a constrained optimisation problem, in which the goal is to stay close to the given primitive, while fulfilling a set of constraints. We show how common adaptation problems in robotics, like respecting joint limits, avoiding obstacles, confining a robot within virtual walls, or combining multiple primitives in the same workspace can be

F. Frank, A. Paraschos, P. v.d. Smagt and B. Cseke are with the Volkswagen Machine Learning Research Lab, Munich, 80805 Germany e-mail: felix.frank@argmax.ai.

A supplementary video can be found at <https://youtu.be/ErdP7bA11v8>.

implemented with constraints. Throughout the adaptation we retain the probabilistic characteristics and synthesise a new primitive, which can then be reproduced on a robot using the known ProMP framework.

We structure the paper as follows: In Section II we give a short introduction to probabilistic movement primitives, followed by the problem formulation. Afterwards we develop several adaptation techniques using probabilistic constraints. Section III presents several applications of our method and we compare our method to previous approaches in Section IV. Finally we conclude the paper and sketch future research directions.

II. METHODOLOGY

In this section we derive our adaptation framework for ProMPs and we propose several constraints which can be used to adapt a primitive to a new situation. We start with the background on ProMPs.

A. Background: Probabilistic Movement Primitives

Probabilistic Movement Primitives (ProMPs) [3] are a method to model trajectory distributions, that are extensively used in robotics [17]–[24]. A trajectory $\mathbf{Y} = \{\mathbf{y}_t\}_{t=0}^L$ typically consists of recordings of a robot’s joint space or certain Cartesian coordinates $\mathbf{y}_t \in \mathbb{R}^D$ at times $t_l \in [0, T]$. In this paper we develop models and methods for the joint space coordinates. Applying them to model Cartesian coordinates is straightforward and can be viewed as a simpler special case—we point out the differences at the appropriate places.

The coordinates \mathbf{y}_t are modelled as a linear combination $\mathbf{z}_t(\mathbf{w}) = \mathbf{w}\phi_t$ under the presence of zero-mean Gaussian noise, that is,

$$\mathbf{y}_{t_l} = \mathbf{z}_{t_l}(\mathbf{w}) + \epsilon_{t_l}, \quad \epsilon_{t_l} \sim \mathcal{N}(0, \Sigma_y). \quad (1)$$

The vector $\phi(t) = [\phi^1(t), \phi^2(t), \dots, \phi^M(t)] \in \mathbb{R}^M$ consists of the values at time t of M basis functions, whereas $\mathbf{w} \in \mathbb{R}^{D \times M}$ is a stochastic weight matrix with the same number of rows D as \mathbf{y}_t . As a result, the observation model is given by

$$p(\mathbf{y}_t | \mathbf{w}) = \mathcal{N}(\mathbf{y}_t; \mathbf{w}\phi_t, \Sigma_y). \quad (2)$$

The distribution over weights $p(\mathbf{w})$ is chosen to be Gaussian, i.e., $p(\mathbf{w}) = \mathcal{N}(\text{vect}(\mathbf{w}); \text{vect}(\boldsymbol{\mu}_w), \Sigma_w)$, where $\text{vect}(\mathbf{w})$ and $\text{vect}(\boldsymbol{\mu}_w)$ are blocked column vectors w.r.t. the rows of \mathbf{w} and $\boldsymbol{\mu}_w$, respectively. For reasons of notational brevity, in the following we use $p(\mathbf{w}) = \mathcal{N}(\mathbf{w}; \boldsymbol{\mu}_w, \Sigma_w)$. The marginal distribution of a trajectory $\mathbf{y}_{0:T}$ can thus be written as

$$p(\mathbf{y}_{0:T} | \boldsymbol{\theta}) = \int \mathcal{N}(\mathbf{w}; \boldsymbol{\mu}_w, \Sigma_w) \prod_{l=1}^L \mathcal{N}(\mathbf{y}_{t_l}; \mathbf{w}\phi_{t_l}, \Sigma_y) d\mathbf{w}, \quad (3)$$

where $\boldsymbol{\theta} = \{\boldsymbol{\mu}_w, \Sigma_w, \Sigma_y\}$ denotes all learnable model parameters.

In robotics, one typically records joint space position and velocity at discrete points in time. The basis functions ϕ_t^i are commonly chosen as Gaussian radial basis functions $\phi_t^i = \exp(-(\tau(t) - c_i)^2 / (2h))$, where the phase variable $\tau(t)$ is a mapping from recorded time to the interval $[0, 1]$. Scaling time

to a common phase space enables using trajectories of different length in one primitive. Additionally, the phase variable allows the adaptation of the execution speed later on. The radial basis functions are chosen because they are localised in time and are infinitely differentiable.

Given a set of trajectories $\{\mathbf{Y}^i\}_{i=1}^n$, which are considered to be i.i.d., one can learn the distribution over weights by maximum likelihood estimation, i.e.,

$$\boldsymbol{\theta}^* = \text{argmax}_{\boldsymbol{\theta}} \sum_i \log p(\mathbf{y}_{0:T}^i | \boldsymbol{\theta}). \quad (4)$$

The maximisation can be carried out with an *Expectation Maximisation* (EM) algorithm that iterates through the E and M steps until convergence is achieved. In the E-step the individual posteriors $p(\mathbf{w} | \mathbf{y}^i, \boldsymbol{\theta}_s) \propto p(\mathbf{y}^i | \mathbf{w}, \boldsymbol{\theta}_s) p(\mathbf{w} | \boldsymbol{\theta}_s)$ are computed, while in the M-step a Gaussian $p(\mathbf{w} | \boldsymbol{\theta}_{s+1})$ that matches the moments of $\frac{1}{n} \sum_i p(\mathbf{w} | \mathbf{y}^i, \boldsymbol{\theta}_s)$ is fitted to update the parameter $\boldsymbol{\theta}$. In many practical applications it is useful to add an additional penalty term $\log p(\boldsymbol{\theta})$ to the objective in (4) and thus resort to maximum a posteriori estimation. A common choice for $p(\boldsymbol{\theta})$ is $p(\boldsymbol{\theta}) = p(\boldsymbol{\mu}_w) p(\Sigma_w) p(\Sigma_y)$ with a Gaussian $p(\boldsymbol{\mu}_w)$ and an inverse-Wishart $p(\Sigma_w)$ and $p(\Sigma_y)$, see [20] and [22]. This regularisation can be particularly important if a subsequent adaptation of the ProMP requires a more flexible function class than the ProMP would and thus one runs the danger of overfitting the data when learning the ProMP.

The distribution $p(\mathbf{w} | \boldsymbol{\theta}^*)$ encodes the probabilistic model learnt from the set of trajectories $\{\mathbf{Y}^i\}_{i=1}^n$, thereby capturing the inherent variability. As a result, ProMPs can be used to generate trajectories similar to $\{\mathbf{Y}^i\}_{i=1}^n$ and also to generalise and explore new interesting trajectories, see example in Section III-C. Moreover, we can rely on the stochastic ProMP controller to reproduce these trajectories on a physical system [3]. In the context of learning from demonstrations, the trajectories $\{\mathbf{Y}^i\}_{i=1}^n$ are typically provided by a human expert.

An important aspect of modelling with ProMPs is adapting the learned primitives to new situations. Previous approaches use, for example, Gaussian conditioning to incorporate via- or end-points in joint space [3] or task space [22]. Other features include merging different primitives [3] or incorporating obstacle avoidance into a trajectory [17]–[19]. In the following we propose a generic framework for ProMPs by constraining the probability mass associated with undesirable trajectories to be low.

B. Adaptation by Trajectory Constraints

Due to the Gaussian nature of the ProMP distribution $p(\mathbf{w})$ the trajectory $\{\mathbf{z}_t\}$, $t \in [0, T]$ is a Gaussian process with mean value function $\mathbb{E}[\mathbf{z}_t] = \boldsymbol{\mu}_w \phi_t$ and covariance function $\text{Cov}[\mathbf{z}_t^i, \mathbf{z}_{t'}^j] = \phi_t^T \Sigma_w^{(i,j)} \phi_{t'}$, where $\Sigma_w^{(i,j)}$ is the covariance matrix block between the rows \mathbf{w}_i and \mathbf{w}_j of \mathbf{w} . Therefore, any finite dimensional joint distribution of $\{\mathbf{z}_t\}$ is also Gaussian and can be easily computed. We define $\{\mathbf{x}_t\}$, with $\mathbf{x}_t(\mathbf{w}) \equiv \mathbf{T}(\mathbf{z}_t(\mathbf{w}))$, as the process corresponding to certain Cartesian coordinates of interest, such as end-effector or elbow pose or velocity. The function \mathbf{T} maps the robot’s joint state

\mathbf{z}_t to the Cartesian coordinates \mathbf{x}_t and it is commonly referred to as the forward kinematics function [25]. When modelling in the Cartesian space we simply set \mathbf{T} to the identity function, that is, $\mathbf{x}_t(\mathbf{w}) \equiv \mathbf{z}_t(\mathbf{w})$.

Generally, in any given robotics task, we have a set of points of interest $\mathbf{x}_t^k(\mathbf{w})$ (see for example Section III-D) and corresponding forward kinematics functions \mathbf{T}_k . Without loss of generality and for reasons of notational brevity we limit our presentation to a single point of interest $\mathbf{x}_t(\mathbf{w})$.

Since $\{\mathbf{z}_t\}$ is a well defined stochastic process, we can express trajectory constraints in terms of probabilities. That is, we can associate a probability mass to a trajectory constraint $c(\{\mathbf{z}_t(\mathbf{w})\}) \leq d$ being valid. For example an end-point constraint $\mathbf{z}_T(\mathbf{w}) \leq d$ being valid with confidence α can be formulated as $P_{\mathbf{w}}(\mathbf{z}_T(\mathbf{w}) \leq d) \geq \alpha$. Here $c(\{\mathbf{z}_t(\mathbf{w})\}) = \mathbf{z}_T(\mathbf{w})$ and $P_{\mathbf{w}}$ denotes the measure corresponding to $p(\mathbf{w})$.

In this paper we consider two types of constraints. First *point constraints* that take as input \mathbf{x}_t or \mathbf{z}_t , such as via- or end-point constraints, and second *path constraints* that are applied to the path $\{\mathbf{x}_t\}_{t \in \mathcal{T}}$ or $\{\mathbf{z}_t\}_{t \in \mathcal{T}}$ with contiguous temporal support $\mathcal{T} \subseteq [0, T]$. For example, bounding the smoothness of a trajectory can be considered a *path constraint*. Generally, we formulate K *point constraints* as inequality constraints $P_{\mathbf{w}}(c_{k,t}(\mathbf{x}_t(\mathbf{w})) \leq d_{k,t}) \geq \alpha_{k,t}$ that are required to be valid at time-point t , whereas *path constraints* are formulated as $P_{\mathbf{w}}(c_k(\{\mathbf{x}_t(\mathbf{w})\}_{t \in \mathcal{T}}) \leq d_k) \geq \alpha_k$, $k \in \{1, \dots, K\}$. While not all these quantities are analytically tractable, for the constraints we consider in this paper we provide accurate approximations that lead to state of the art results.

C. Problem Formulation

As we discussed in the previous section, ProMPs represent the information learnt from the trajectories $\{\mathbf{Y}^i\}_{i=1}^n$ with a Gaussian distribution which we now denote by $p_0(\mathbf{w}) = \mathcal{N}(\mathbf{w}; \boldsymbol{\mu}_w^0, \boldsymbol{\Sigma}_w^0)$. In this paper we view adaptation as imposing constraints on the paths generated by this distribution. In this view, adaptation means computing a new $p(\mathbf{w})$ which is as close as possible to $p_0(\mathbf{w})$, while paths generated from $p(\mathbf{w})$ satisfy a set of constraints. We formulate the adaptation of ProMPs as the constrained optimisation problem,

$$\min_p D_{\text{KL}}[p(\mathbf{w}) \| p_0(\mathbf{w})] \quad (5a)$$

$$\text{s.t. } E_{p(\mathbf{w})}[H(d_{k,t} - c_{k,t}(\mathbf{w}))] \geq \alpha_{k,t} \quad \forall k, t \in \mathcal{T}_k, \quad (5b)$$

where we rewrite the probability mass constraints as expectation constraints

$$P_{\mathbf{w}}(c_{k,t}(\mathbf{w}) \leq d_{k,t}) = E_{p(\mathbf{w})}[H(d_{k,t} - c_{k,t}(\mathbf{w}))]. \quad (6)$$

The function H stands for the heavyside step function and the set \mathcal{T}_k denotes the temporal support of the k^{th} constraint. For example, for an end-point constraint we have $\mathcal{T}_k = \{T\}$, while when limiting the end-effector trajectories to a predefined area for a certain time we have $\mathcal{T}_k \subseteq [0, T]$, see examples in Figure 1 and Section III-A1. The objective in equation (5a) is the (reverse) Kullback-Leibler divergence. We choose this divergence because its analytical tractability w.r.t. the Gaussian family of distributions and because of its mode-seeking property [26] when compared to $D_{\text{KL}}[p_0(\mathbf{w}) \| p(\mathbf{w})]$.

The latter property is particularly important because, as we shall see later, the distributions carved out by the constraints are often highly multimodal. In this formulation, without lack of generality, we omit the dependence of $c_{k,t}$ on either $\mathbf{x}_t(\mathbf{w})$ or $\mathbf{z}_t(\mathbf{w})$ because all the stochasticity in the model is captured by the variable \mathbf{w} . Note that there should be an additional normalisation constraint for p ; for notational brevity, we omit this because it can be easily included in the formulation. Furthermore, *path constraints* can be added by imposing $E_{p(\mathbf{w})}[H(d_k - c_k(\mathbf{w}))] \geq \alpha_k$, see Section II-D2.

Alternatively, instead of imposing strict limits, we can relax constraints and recast them as penalties which we add to the objective (5a). For example, adding a smoothness regulariser $R(\{\mathbf{z}_t(\mathbf{w})\})$ leads to a trade-off of staying close to the given prior and prioritising smooth trajectories. To achieve this, one can add $\kappa E_{p(\mathbf{w})}[R(\mathbf{w})]$ to the objective (5a).

The constrained optimisation problem in (5a) and (5b) is a convex problem with linear constraints w.r.t. $p(\mathbf{w})$. The corresponding Lagrangian reads as

$$L(p, \{\lambda_{k,t}\}) = D_{\text{KL}}[p(\mathbf{w}) \| p_0(\mathbf{w})] \quad (7)$$

$$+ \sum_{k,t} \lambda_{k,t} [\alpha_{k,t} - E_{p(\mathbf{w})}[H(d_{k,t} - c_{k,t}(\mathbf{w}))]]$$

and the resulting optimisation problem is formulated as

$$\max_{\lambda_{k,t} \geq 0} \min_p L(p, \{\lambda_{k,t}\}). \quad (8)$$

The optimisation problem is convex-concave in p and $\{\lambda_{k,t}\}$ and the optimal $(p^*, \{\lambda_{k,t}^*\})$ yields

$$p^*(\mathbf{w}) \propto p_0(\mathbf{w}) \exp \left\{ \sum_{k,t} \lambda_{k,t}^* H(d_{k,t} - c_{k,t}(\mathbf{w})) \right\}. \quad (9)$$

This distribution is non Gaussian, non-smooth, and often multimodal. However, we are interested in finding a Gaussian $p^*(\mathbf{w})$ to be able to keep the ProMP formulation and, subsequently, its properties. Additionally, keeping the ProMP formulation allows us to use a known stochastic controller that can reproduce the trajectory distribution on a physical system [3]. For this reason, in the following we restrict the search space of $p(\mathbf{w})$ to Gaussians and we use the mode-seeking KL divergence in (5a) to find a relevant mode and the corresponding optimum.

Let $p(\mathbf{w}) = \mathcal{N}(\mathbf{w}; \boldsymbol{\mu}_w, \boldsymbol{\Sigma}_w)$ and let $F_{c_{k,t}}(\cdot; \boldsymbol{\mu}_w, \boldsymbol{\Sigma}_w)$ denote the cumulative distribution function of the random variable defined by $c_{k,t}(\mathbf{w})$. With this parameterisation the constraints are typically no longer convex, however, in most cases reasonably good saddle-points can be found by gradient ascent-descent methods. The Lagrangian resulting from this parameterisation can be written as

$$L(\boldsymbol{\mu}_w, \boldsymbol{\Sigma}_w, \{\lambda_{k,t}\}) = D_{\text{KL}}[\mathcal{N}(\mathbf{w}; \boldsymbol{\mu}_w, \boldsymbol{\Sigma}_w) \| \mathcal{N}(\mathbf{w}; \boldsymbol{\mu}_w^0, \boldsymbol{\Sigma}_w^0)]$$

$$+ \sum_{k,t} \lambda_{k,t} [\alpha_{k,t} - F_{c_{k,t}}(d_{k,t}; \boldsymbol{\mu}_w, \boldsymbol{\Sigma}_w)]. \quad (10)$$

In the following we use this latter formulation to adapt ProMPs to new scenarios. We formulate every adaptation in a generic way by defining the corresponding $c_{k,t}(\mathbf{w})$ and approximating its cumulative distribution function $F_{c_{k,t}}$. Moreover, we use

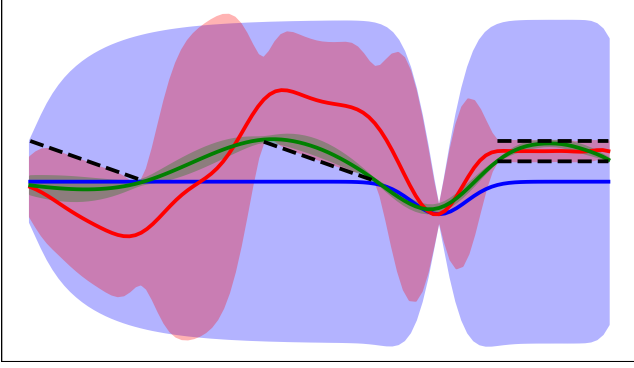


Fig. 1. A toy example illustrating limit constraints (dashed, black lines) and the effects of the smoothness regulariser introduced in Section II-D. The wide Gaussian prior (blue) is adapted to obey limit constraints (red). A smoother distribution of trajectories with lower variance is obtained when smoothness regulariser ($\kappa = 0.01$) is added (green). The thick line corresponds to the mean of the respective primitive, whereas the shaded area indicates three standard deviations.

differentiable approximations so that the gradients of the Lagrangian can be numerically computed using automatic differentiation frameworks.

D. Joint space constraints

These constraints depend directly on $\{z_t(\mathbf{w})\}$ and hence their computation does not involve an often non-linear forward kinematics function.

1) *Limits on joint space coordinates:* In general every robotic movement is limited to a specific motion range depending on the robot's links and their configuration. These limits can also change during operation, for example, we might want to limit the range of motion of a link after a failure, or when newly added sensor blocks part of the motion range. Changing these limits requires an adaptation of the learned movement primitives. For dynamic movement primitives the problem of joint limit avoidance has been addressed by learning primitives in a transformed space [10]. However, this method requires demonstrations to already conform to the limits, otherwise a mapping of demonstrations to the transformed space is not straightforward. In our probabilistic framework, we can add constraints to an existing trajectory distribution. A one-sided constraint can be formulated as

$$P_{\mathbf{w}}(z_t^k(\mathbf{w}) \leq b_{k,t}) \geq \alpha_{k,t}, \quad (11)$$

while for a two-sided constraint we can use

$$P_{\mathbf{w}}(a_{k,t} < z_t^k(\mathbf{w}) \leq b_{k,t}) \geq \alpha_{k,t}. \quad (12)$$

In this case, instead of the step function $H(\cdot)$, we can use the indicator function $I_{D_{k,t}}(\cdot)$ of the interval $D_{k,t} = [a_{k,t}, b_{k,t}]$ to formulate the probability mass constraint as an expectation constraint. The latter can then be added to (5b) by using

$$E[I_{D_{k,t}}(z_t^k)] = \Phi \left[\frac{b_{k,t} - E[z_t^k]}{V[z_t^k]^{1/2}} \right] - \Phi \left[\frac{a_{k,t} - E[z_t^k]}{V[z_t^k]^{1/2}} \right], \quad (13)$$

with Φ denoting the CDF of a standard normal random variable. Note that these constraints only satisfy the joint limits in the probabilistic sense, that is, the probability of being out

of bounds is very low. Nonetheless, this method can be used to adapt to changing operational conditions, whereas for simple joint limit avoidance one should rely on learning the movement primitives in a transformed space, analogous to [10], resulting in stronger guarantees.

In Figure 1 we illustrate a toy adaptation problem for a univariate ProMP with time-varying one-sided and fixed two-sided limit constraints. The original ProMP is a wide non-informative Gaussian with a via-point computed by conditioning. The adapted ProMP conforms both to the boundary constraints and the restrictive original ProMP at the via-point.

2) *Smoothness constraints:* In many applications the smoothness of the trajectory is an important factor to take into account because smooth trajectories are easier to control and they typically consume less energy. For this reason, we consider imposing constraints on or regularising with the 2-norm of the 2^{nd} time derivative of the joints' trajectory. This is a commonly used spline smoothing regularisation [27] and can be viewed as Bayesian estimation with a Gaussian process prior where the covariance function is determined by the 2^{nd} order differential operator [28]. As a result, we can view the original process $\{z_t\}_{t \in [0, T]}$ as a Gaussian process with a covariance function that is a combination of the covariance functions corresponding to the ProMP and the smoothing regulariser.

To simplify notation, we present the derivation for a scalar trajectory. A smoothness regulariser can be formulated as

$$R(\{z_t\}) = \frac{1}{|\mathcal{T}|} \int_{\mathcal{T}} |z_t''|^2 dt$$

which in the context of ProMPs results in the quadratic form

$$R(\mathbf{w}) = \mathbf{w}^T \left[\frac{1}{|\mathcal{T}|} \int_{\mathcal{T}} [\phi_t''] [\phi_t'']^T dt \right] \mathbf{w}. \quad (14)$$

We can either add $P_{\mathbf{w}}(R(\mathbf{w}) \leq d) \geq \alpha$ as a constraint to (5b) or relax it to a regulariser $\kappa E_{p(\mathbf{w})}[R(\mathbf{w})]$ to be added to the objective in (5a).

The distribution of the random variable $R(\mathbf{w})$ is a generalised- χ^2 and due to positive semi-definiteness of the interaction matrix in (14), we have $R(\mathbf{w}) \geq 0$. Since the CDF has an intricate numerical form, we approximate $R(\mathbf{w})$ with a simpler Gamma distribution that matches its mean and variance, that is, we use $R(\mathbf{w}) \sim \Gamma(\alpha, \beta)$ with shape $\alpha = E[R(\mathbf{w})]^2 / V[R(\mathbf{w})]$ and rate $\beta = E[R(\mathbf{w})] / V[R(\mathbf{w})]$. By denoting with Φ the matrix of the quadratic form in (14)—which we compute by numerical integration—we find that

$$E[R(\mathbf{w})] = \boldsymbol{\mu}_w^T \Phi \boldsymbol{\mu}_w + \text{tr}(\Phi \boldsymbol{\Sigma}_w) \quad (15)$$

$$V[R(\mathbf{w})] = 4\boldsymbol{\mu}_w^T \Phi \boldsymbol{\Sigma}_w \Phi \boldsymbol{\mu}_w + 2\text{tr}(\Phi \boldsymbol{\Sigma}_w \Phi \boldsymbol{\Sigma}_w).$$

In Figure 1 we illustrate the effect of a smoothness regulariser $\kappa E_{p(\mathbf{w})}[R(\mathbf{w})]$ in a toy adaptation problem: the smoothness regularisation results in a trajectory distribution with a significantly reduced variance and a mean function that gets close to the constraint limits to increase smoothness. The significant reduction of variance is due to (15): by using $\Phi = \mathbf{U}_{\Phi} \text{diag}(\lambda_{\Phi}^i) \mathbf{U}_{\Phi}^T$ and writing $\boldsymbol{\Sigma}_w = \mathbf{U}_{\Phi} \boldsymbol{\Sigma}_{\Phi} \mathbf{U}_{\Phi}^T$ we find that $\text{tr}(\Phi \boldsymbol{\Sigma}_w) = \sum_i \lambda_{\Phi}^i \boldsymbol{\Sigma}_{\Phi}^{ii}$. Since we have $\text{tr}(\boldsymbol{\Sigma}_w) = \text{tr}(\boldsymbol{\Sigma}_{\Phi}) = \sum_i \boldsymbol{\Sigma}_{\Phi}^{ii}$, we can conclude that (15) incentivises

small overall variances. While the KL objective in (5a) is trying to keep both the mean $\boldsymbol{\mu}_w$ and covariance $\boldsymbol{\Sigma}_w$ close to the original ProMP's mean and covariance, the expression in (15) prefers $\boldsymbol{\mu}_w$ with (generally) smaller norms and covariances $\boldsymbol{\Sigma}_w$ with smaller overall variance. As a result, by adding a smoothness regularisation, we express preference towards a small set of smooth trajectories from the ones defined by the original ProMP.

E. Task space constraints

It is equally important to formulate constraints on the Cartesian position of robot parts, like the end-effector, the elbow or any other point of interest determined by robot's joints' configuration. Previous work used the probabilistic conditioning methods to adapt primitives in a table tennis setting with via-points [21] and showed how obstacle avoidance can be achieved with policy search [17], constrained optimisation [18] and movement planning [19]. Our approach offers a generic way to incorporate limits on the robot's Cartesian coordinates by formulating constraints in terms of the process $\{\mathbf{x}_t\}$. Given a constraint $c_{k,t}(\mathbf{x}_t(\mathbf{w}))$, we approximate the distribution of the random variable $c_{k,t}(\mathbf{w}) = c_{k,t}(\mathbf{T}(z_t(\mathbf{w})))$ with a distribution from a known family of distributions. In cases where \mathbf{T} or c_k introduce nonlinear dependencies we use the *Unscented Transform* [29] to do moment-based approximations. When modelling in the Cartesian space, \mathbf{T} is the identity function, hence the *Unscented Transform* is not necessary.

The *Unscented Transform* is a sample based method for computing statistics of a nonlinear transformation $\mathbf{g}(z_S)$ of the random variable z_S , $S \subseteq [0, T]$. Given z_S with mean $\mathbb{E}[z_S]$ and variance $V[z_S]$, one selects $2D+1$ specific sample points $\bar{z}_m = \mathbb{E}[z_S] \pm (\alpha\sqrt{DV[z_S]})_m$ and weights $W_m = 1/(2(\alpha^2 D))$ to estimate the mean and the variance as

$$\begin{aligned} \mathbb{E}[\mathbf{g}(z_S)] &\approx \sum_m W_m \mathbf{g}(\bar{z}_m) \\ V[\mathbf{g}(z_S)] &\approx \sum_m W_m [\mathbf{g}(\bar{z}_m) - \mathbb{E}[\mathbf{g}(z_S)]] [\mathbf{g}(\bar{z}_m) - \mathbb{E}[\mathbf{g}(z_S)]]^T \end{aligned}$$

Here, the parameter α determines the spread of the sample points around the mean. Depending on the type of constraint, we use the unscented transform either to approximate $\mathbf{x}_S(\mathbf{w}) = \mathbf{T}(z_S(\mathbf{w}))$ or $c_k(z_S(\mathbf{w}))$ directly.

In the following we introduce different task space constraints. We demonstrate most of these in small, dedicated experiments with a planar robot in Section III-A and we encourage readers to cross check the respective experiments for a visual interpretation of the individual effects.

1) *Hyperplane constraints*: In a production setting robots are usually confined to their own workspace often delimited by fences. We can formulate virtual wall constraints as

$$P_w(\mathbf{n}_{k,t}^T(\mathbf{x}_t(\mathbf{w}) - \mathbf{b}_{k,t}) \leq 0) \geq \alpha_{k,t} \quad (16)$$

where $\mathbf{n}_{k,t}$ and $\mathbf{b}_{k,t}$ denote the normal and bias vectors of a hyperplane. As a result, we have to estimate the distribution of the random variable $c_{k,t}(\mathbf{w}) = \mathbf{n}_{k,t}^T(\mathbf{x}_t(\mathbf{w}) - \mathbf{b}_{k,t})$, which is a linear transformation of $\mathbf{x}_t(\mathbf{w})$. However, $\mathbf{x}_t(\mathbf{w})$ is non-linear in \mathbf{w} thus we use the unscented transform to approximate

$\mathbf{x}_t(\mathbf{w}) = \mathbf{T}(z_t(\mathbf{w}))$ with a Gaussian $\tilde{\mathbf{x}}_t(\mathbf{w}) \approx \mathbf{T}(z_t(\mathbf{w}))$. This leads to the Gaussian approximation

$$c_{k,t}(\mathbf{w}) \sim \mathcal{N}(\mathbf{n}_{k,t}^T(\mathbb{E}[\tilde{\mathbf{x}}_t(\mathbf{w})]) - \mathbf{b}_{k,t}, \mathbf{n}_{k,t}^T V[\tilde{\mathbf{x}}_t(\mathbf{w})] \mathbf{n}_{k,t}).$$

In this instance we set $d_{k,t} = 0$ and we use the corresponding Gaussian CDF in (10).

Note that although our approach allows for time-varying parameters, in most common settings both $\mathbf{n}_{k,t}$ and $\mathbf{b}_{k,t}$ are constant in time and the constraints are required to be valid throughout the whole trajectory, that is, $\mathcal{T}_k = [0, T]$. Using several *hyperplane constraints* we can confine the trajectories to more complex convex domains. We do this by requiring the satisfaction of the constraint for each individual hyperplane.

2) *Waypoints and repellers*: In many applications we would like the trajectory of robot links or, more generally, any point of interest on the robot $\mathbf{x}_t(\mathbf{w})$, to be close to (waypoint) or to avoid (repeller) certain points $\bar{\mathbf{x}}_t$ in the task space. We formulate such trajectory constraints by

$$P_w(|\mathbf{x}_t(\mathbf{w}) - \bar{\mathbf{x}}_t|^2 \leq d^2) \geq \alpha_t \quad (17)$$

for waypoints and by

$$P_w(|\mathbf{x}_t(\mathbf{w}) - \bar{\mathbf{x}}_t|^2 > d^2) \geq \alpha_t \quad (18)$$

for repellent points. Depending on the choice of \mathcal{T} , these constraints can be used to implement end-point constraints $\mathcal{T} = \{T\}$, obstacle avoidance $\mathcal{T} = [0, T]$ or other constraints with more interesting temporal support $\mathcal{T} \subset [0, T]$ (see for example Section III-A1).

To integrate these types of constraints into our framework we need to approximate the distribution of the random variable $c_{k,t}(\mathbf{w}) = |\mathbf{x}_t(\mathbf{w}) - \bar{\mathbf{x}}_t|^2$. To approximate $c_{k,t}(\mathbf{w})$ we use a Gamma approximation similar to the smoothness constraint in Section II-D2. The mean $\mathbb{E}[c_{k,t}(\mathbf{w})]$ and the variance $V[c_{k,t}(\mathbf{w})]$ are approximated using the unscented transform for $c_{k,t}(\mathbf{w})$. Depending on whether we have a waypoint or a repellent point we use the corresponding complementary values of the CDF of the resulting Gamma distribution.

3) *Temporally unbound waypoints*: In some applications one might not want to fix the time point of the waypoint, instead only constrain the trajectory to visit a point in task space or joint space at an unspecified time point—see example in Section III-D. We can formalise this as

$$\max_{t \in \mathcal{T}} P_w(|\mathbf{x}_t(\mathbf{w}) - \bar{\mathbf{x}}|^2 \leq d^2) \geq \alpha, \quad \mathcal{T} \subseteq [0, T] \quad (19)$$

that is, we require that there exists a time point $t_{\max} \in \mathcal{T}$ at which the waypoint constraint is satisfied with confidence α . The r.h.s. of (19) is analytically intractable, however, its computation is algorithmically feasible since we can select $t_{\max} = \operatorname{argmax}_{t \in \mathcal{T}} P_w(|\mathbf{x}_t(\mathbf{w}) - \bar{\mathbf{x}}|^2 \leq d^2)$ when using the corresponding approximation for $P_w(|\mathbf{x}_t(\mathbf{w}) - \bar{\mathbf{x}}|^2 \leq d^2)$. Note that similarly to the *smoothness constraint* this constraint is a *path constraint* as the r.h.s. depends on the path $\{\mathbf{x}_t\}_{t \in \mathcal{T}}$.

4) *Non-convex domains*: With the hyperplane constraints in mind, we can also consider tackling the problem of obstacles with a piecewise linear volume, i.e., not spheres as in the case

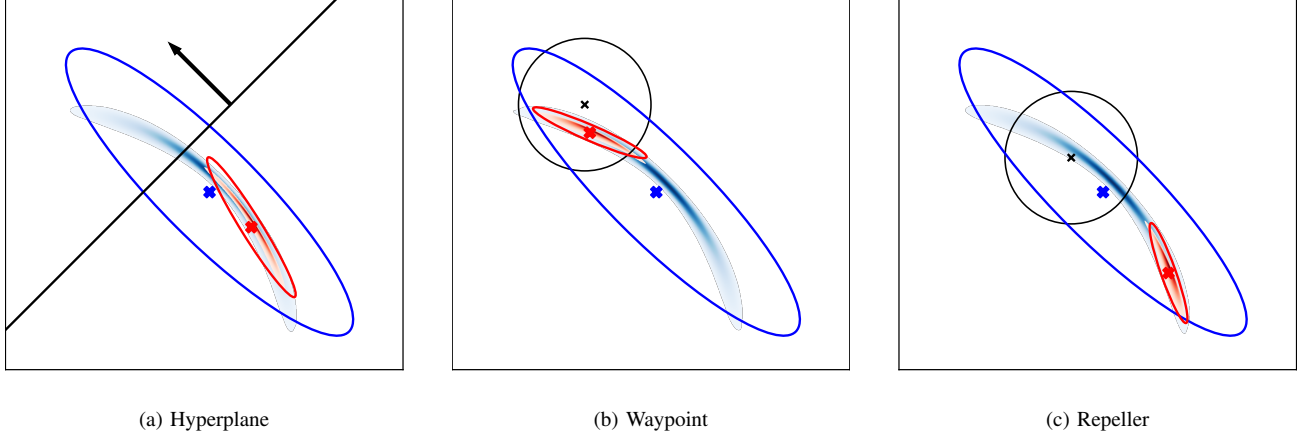


Fig. 2. Approximations using the *Unscented Transform*. The panels of the figure show how the *unscented transform* based approximation works for a variety of constraints when using the forward kinematics function of a planar robot. The heatmaps show the original (blue) and the adapted (red) distribution of $\mathbf{x}_t(\mathbf{w})$ while the ellipsis show the Gaussians corresponding to their respective mean and covariance (0.95-level sets).

of repellers. Specifically, we imagine the corner or a box that is to be avoided. We can formulate this constraint as

$$P_{\mathbf{w}}(\mathbf{n}_{1,t}^T(\mathbf{x}_t - \mathbf{b}_{1,t}) \geq 0 \wedge \mathbf{n}_{2,t}^T(\mathbf{x}_t - \mathbf{b}_{2,t}) \geq 0) \leq 1 - \alpha_t. \quad (20)$$

which can be expressed as the expectation constraint

$$E_{p(\mathbf{w})}[H(\mathbf{n}_{1,t}^T(\mathbf{x}_t - \mathbf{b}_{1,t})) \cdot H(\mathbf{n}_{2,t}^T(\mathbf{x}_t - \mathbf{b}_{2,t}))] \leq 1 - \alpha_t. \quad (21)$$

Computing this expectation is generally an analytically intractable problem. Hence we approximate the expectation of the product in (21) with a product of expectations. This results in approximating (20) with

$$P_{\mathbf{w}}(\mathbf{n}_{1,t}^T(\mathbf{x}_t - \mathbf{b}_{1,t}) \geq 0) P_{\mathbf{w}}(\mathbf{n}_{2,t}^T(\mathbf{x}_t - \mathbf{b}_{2,t}) \geq 0) \leq 1 - \alpha_t.$$

This approximation is exact when $\mathbf{n}_{1,t}^T \mathbf{n}_{2,t} = 0$, that is, the two hyperplanes are orthogonal to each other and either of the following conditions hold (i) $V[\mathbf{x}_t]$ is diagonal or (ii) its eigenvectors are perpendicular to $\mathbf{n}_{1,t}$ and $\mathbf{n}_{2,t}$. The expression in equation (21) can be integrated in our framework by using the approach derived for approximating (16).

For arbitrary non-convex domains, however, one might have to derive approximations on a case by case basis. A generic approach can be to find an optimal approximate spherical cover of the domain or its boundary, that is, a collection of spheres the union of which contain the domain, and use the corresponding collection of repellers for adaptation. Another approach is to define a collection of time-dependent tangent hyperplane constraints with limited, say, a sliding window based, temporal support—in this case, however, the adaptation will be dependent on our choice for the constraints' temporal support or the constraints' parameters will depend on the robot's state. Generally, a wide variety of domains (or their boundary) can be approximated by using an optimal arrangement of repellers and hyperplanes and their temporal support, thus our approach can be used to constrain trajectories to lie within or to avoid such domains. We will address this in a future work.

5) *Mutual (self) avoidance*: A common scenario where adaptation plays an important role is when several robots operate at the same time in a confined space. Let us consider the simple scenario when we would like two robots to execute independently learned ProMPs, however, we would also like them to avoid collision of their end-effectors or points of interest. We can formulate this simple adaptation problem as follows. Let $p_0(\mathbf{w}_1, \mathbf{w}_2) = p_0(\mathbf{w}_1) p_0(\mathbf{w}_2)$ be the joint ProMP corresponding to the independently learned ProMPs of two robots and let us assume that we have two Cartesian points of interest $\mathbf{x}_t^1(\mathbf{w}_1)$ and $\mathbf{x}_t^2(\mathbf{w}_2)$ —one on each robot—that should not collide. We can formulate this adaptation problem as learning a new joint ProMP $p(\mathbf{w})$ with $\mathbf{w} = (\mathbf{w}_1, \mathbf{w}_2)$ such that

$$P_{\mathbf{w}}(|\mathbf{x}_t^1(\mathbf{w}_1) - \mathbf{x}_t^2(\mathbf{w}_2)|^2 > d^2) \geq \alpha_t. \quad (22)$$

We consider two options for the objective: (i) the Kullback-Leibler divergence $D_{\text{KL}}[p(\mathbf{w}_1, \mathbf{w}_2) \| p_0(\mathbf{w}_1) p_0(\mathbf{w}_2)]$ between the jointly adapted ProMP and the joint distribution of the original ProMPs and (ii) the sum of marginal Kullback-Leibler divergences $D_{\text{KL}}[p(\mathbf{w}_1) \| p_0(\mathbf{w}_1)] + D_{\text{KL}}[p(\mathbf{w}_2) \| p_0(\mathbf{w}_2)]$. The first objective favours adapted joint distributions that are similar to the factorising original distribution and thus penalises high covariance between \mathbf{w}_1 and \mathbf{w}_2 —beyond what is necessary to satisfy the avoidance constraints, The second objective is more agnostic about the covariances and only focuses on the adapted marginal distributions being similar to the two original ProMPs.

In the planar robot toy experiment in Section III-A5 we visualize the effect of the two objectives on the covariances. This approach can be generalised to several robots and several points of interest required in practical applications. In Section III-D we apply mutual avoidance with several points of interest in real world dual arm setting.

In this section we have presented a collection of constraints, and corresponding approximations, that enable us to apply the ProMP adaptation method we introduced in Section II-C to a large variety of adaptation problems. In the following we

present the technical details of the Lagrangian optimisation, readers more interested in applications can skip to Section III.

F. Combining movement primitives

Combining movement primitives is an important topic in the Learning from Demonstrations (LfD) literature. Although it is not the central topic of this paper, since we can always apply adaptation after solving the combination task, it is interesting to see how simple ProMP combinations could be integrated into our framework. There are several ways to combine ProMPs [15], here we only consider distributional geometric combinations. We can combine and adapt K ProMPs $p_i(\mathbf{w})$, $i = 1, \dots, K$ in the joint space by choosing the objective in (5a) as $\sum_i \alpha_i D[p(\mathbf{w}) || p_i(\mathbf{w})]$, where α_i denotes a set of normalised weights. When a ProMP is defined in the Cartesian space we can opt for marginal matching and replace the corresponding term with $(M/3T) \sum_t D[p(\bar{\mathbf{x}}_t(\mathbf{w}) || p_i(\mathbf{x}_t(\mathbf{w}))]$, where the scaling factor $M/3$ accounts for the difference in dimensionality. Here $\bar{\mathbf{x}}_t(\mathbf{w})$ is the approximation of Cartesian point of interest introduced above and $\mathbf{x}_t(\mathbf{w})$ are the Cartesian points of interest of the movement primitive to be combined.

G. Optimisation techniques

The approximation methods for the CDFs corresponding to the various constraints lead to an approximation of the Lagrangian (10) that we optimise using gradient methods. For notational brevity, here we only present the optimisation for simple hyperplane, waypoint, and repeller constraints. Let us use the notation $\boldsymbol{\theta}_0 = (\boldsymbol{\mu}_w^0, \boldsymbol{\Sigma}_w^0)$ for the parameters of the prior $p_0(\mathbf{w})$ and $\boldsymbol{\theta}_k = (\mathbf{n}_k, \mathbf{b}_k)$ and $\boldsymbol{\theta}_k = (\bar{\mathbf{x}}, d)$ for the parameters of the hyperplanes, and repellent/waypoints, respectively. These are fixed during the optimisation. For the parameters of $p(\mathbf{w})$ we use $\boldsymbol{\theta} = (\boldsymbol{\mu}_w, \boldsymbol{\Sigma}_w)$. With this notation, we can write the approximation of the Lagrangian in (10) as

$$\tilde{L}(\boldsymbol{\theta}, \{\lambda_{k,t}\}) = D_{\text{KL}}[\boldsymbol{\theta} || \boldsymbol{\theta}_0] + \sum_{k,t} \lambda_{k,t} \tilde{C}_{k,t}(\boldsymbol{\theta}, \boldsymbol{\theta}_k, \alpha_{k,t}) \quad (23)$$

where we use $\tilde{C}_{k,t}(\boldsymbol{\theta}, \boldsymbol{\theta}_k, \alpha_{k,t}) = \alpha_{k,t} - \tilde{F}_{C_{k,t}}(d_{k,t}; \boldsymbol{\mu}_w, \boldsymbol{\Sigma}_w)$ to denote the corresponding constraint approximation. To solve the optimisation problem corresponding to (8), we use an ascent-descent method which we detail in the following.

The term $D_{\text{KL}}[\boldsymbol{\theta} || \boldsymbol{\theta}_0]$ denotes the Kullback-Leibler divergence between to multivariate Gaussians

$$D_{\text{KL}}[\boldsymbol{\theta} || \boldsymbol{\theta}_0] = -\frac{1}{2}DM - \frac{1}{2} \log |\boldsymbol{\Sigma}_w| + \frac{1}{2} \text{tr}([\boldsymbol{\Sigma}_w^0]^{-1} \boldsymbol{\Sigma}_w) + \frac{1}{2} (\boldsymbol{\mu}_w - \boldsymbol{\mu}_w^0)^T [\boldsymbol{\Sigma}_w^0]^{-1} (\boldsymbol{\mu}_w - \boldsymbol{\mu}_w^0) + \frac{1}{2} \log |\boldsymbol{\Sigma}_w^0|$$

which decouples into two independent terms for $\boldsymbol{\mu}_w$ and $\boldsymbol{\Sigma}_w$ respectively. We use a Cholesky factorisation based parameterisation $\boldsymbol{\Sigma}_w = \mathbf{L}\mathbf{L}^T$, $\mathbf{L} = \mathbf{L}_{\text{tril}} + \text{diag}(\exp(\boldsymbol{\gamma}))$, with \mathbf{L}_{tril} strictly lower triangular, to obtain $\log |\boldsymbol{\Sigma}_w| = \mathbf{1}^T \boldsymbol{\gamma}$ and thus to reduce $D_{\text{KL}}[\boldsymbol{\theta} || \boldsymbol{\theta}_0]$ to a simple analytic form. The factors $\tilde{C}_{k,t}(\boldsymbol{\theta}, \boldsymbol{\theta}_k, \alpha_{k,t})$ involve longer computation chains with numeric algebraic computations. We use automatic differentiation in *Tensorflow* [30] to compute the gradients $\partial_{\boldsymbol{\theta}} \tilde{L}(\boldsymbol{\theta}, \{\lambda_{k,t}\})$ and perform gradient based descent steps.

Algorithm 1 A gradient ascent-descent optimisation algorithm (LBFSGS-EMM) to optimise (8) with the objective (23).

Inputs:

$\boldsymbol{\theta}_0 = (\boldsymbol{\mu}_w^0, \boldsymbol{\Sigma}_w^0)$ ▷ original ProMP
 K constraints with $\boldsymbol{\theta}_k$, $\alpha_{k,t}$, η_k , T_k , τ_k
 • Waypoint/Repeller: $\boldsymbol{\theta}_k = (\bar{\mathbf{x}}_k, d_k)$
 • Hyperplane: $\boldsymbol{\theta}_k = (\mathbf{n}_k, \mathbf{b}_k)$

Outputs:

$\boldsymbol{\mu}_w, \boldsymbol{\Sigma}_w^{1/2} = \mathbf{L}_{\text{TRIL}} + \text{diag}(\exp(\boldsymbol{\gamma}))$

Learnable parameters:

$\boldsymbol{\theta} = (\boldsymbol{\mu}_w, \mathbf{L}_{\text{TRIL}}, \boldsymbol{\gamma}), \{\lambda_{k,t}\}$

Initialisation:

$\boldsymbol{\theta}^0 \leftarrow \boldsymbol{\theta}_0$, $\lambda_{k,t}^0$ (see Section III)

Optimisation:

repeat

repeat

$\boldsymbol{\theta}^{(s+1)} \leftarrow \text{LBFSGS-Step}(\tilde{L}, \partial_{\boldsymbol{\theta}} \tilde{L}, \boldsymbol{\theta}^s, \{\lambda_{k,t}^{(r)}\})$ ▷ Descent

until inner-loop-condition

$\lambda_{k,t}^{(r+1)} \leftarrow \lambda_{k,t}^{(r)} \cdot \exp\{\eta_k \tilde{C}_{k,t}(\boldsymbol{\theta}^s, \boldsymbol{\theta}_k, \alpha_{k,t})\}$ ▷ Ascent

until converged

The optimisation w.r.t. $\lambda_{k,t}$ requires $\lambda_{k,t} \geq 0$. For this we use the Exponential Method of Multipliers (EMM) [31] to perform gradient quasi-ascent steps with $\lambda_{k,t}^{(s+1)} = \lambda_{k,t}^{(s)} \cdot \exp\{\eta_k \partial_{\lambda_{k,t}} \tilde{L}\}$; note that $\partial_{\lambda_{k,t}} \tilde{L} = \tilde{C}_{k,t}$. The latter leads to $\Delta \lambda_{k,t}^{(s)} = \lambda_{k,t}^{(s)} \cdot (\exp\{\eta_k \partial_{\lambda_{k,t}} \tilde{L}\} - 1)$ with $\Delta \lambda_{k,t}^{(s)} \cdot \partial_{\lambda_{k,t}} \tilde{L} \geq 0$, that is, the updates are aligned with the gradient.

To optimise (23) we use a double-loop algorithm: we perform several LBFSGS [32] steps in $\boldsymbol{\theta}$ (*inner-loop*), followed by a *quasi-ascent* step in $\lambda_{k,t}$ with EMM (*outer-loop*). For the *inner-loop* we tried several stopping criteria such as convergence of LBFSGS and consistently increasing constraint violations. We observed that a combination of these two criteria leads to the best overall performance in terms of convergence speed. The optimisation was implemented using the *Tensorflow* automatic differentiation framework. The LBFSGS descent and EMM ascent optimisation is summarised in Algorithm 1.

III. EXPERIMENTAL RESULTS

We validate our approach in two different settings. First, we demonstrate how our proposed adaptation method works through experiments for all constraint types introduced in Section II-E on a simulated, 4-DoF planar robot arm. We then advance to a Franka Emika Panda robot arm with 7 DoF for which we design experiments of increasing difficulty, each of which require several different types of constraints. We start with a single robot arm, and then combine two arms to show the application of the mutual avoidance constraint described in Section II-E5.

A. Experiments on a simulated planar robot arm

In order to demonstrate each task space constraint, we implemented a simple planar robot arm simulator with linear dynamics. The system state consists of the joint positions and

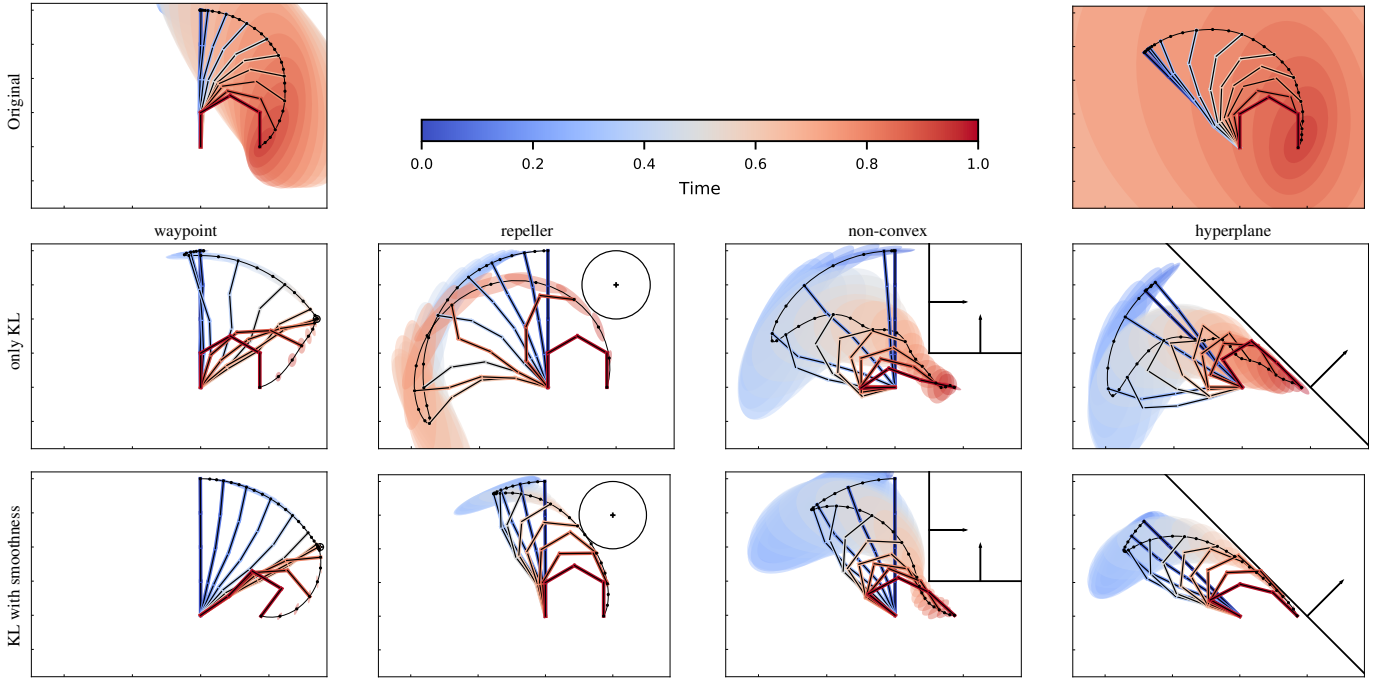


Fig. 3. *Illustrating trajectory adaptation on a planar robot.* The panels in this figure illustrate the examples presented in Section III-A. The colour gradients show time progression. We visualise the mean trajectory and the 0.95 level sets corresponding to the end-effector’s Cartesian space covariances computed using the unscented transform. Note that the covariances are Gaussian approximations to the true distribution of the end-effector position and thus can also show mass outside of the robot’s reach (see also Figure 2). The top row shows the original, unconstrained ProMPs after learning from demonstrations. For the experiments with the waypoint, the repeller and the non-convex constraint these are the same (top-left), whereas the original ProMP for the hyperplane experiment is different and is visualised in the top right panel. The rest of the panels show adaptation for waypoint (left column), repeller (second from left), non-convex (second from right), and hyperplane (right column) constraints; both without (middle row) and with (bottom row) smoothness regularisation added to the objective. See Section III-A for details.

angular velocities while the angular accelerations are directly used as control input. We use the ProMPs to model the joint positions. We use the mean and variance of the Cartesian coordinates corresponding to the adapted ProMP $\mathcal{N}(\mathbf{w}; \boldsymbol{\mu}_w, \boldsymbol{\Sigma}_w)$ to create the illustrations. Sampling trajectories to learn the original (unadapted) ProMP, i.e., $\mathcal{N}(\mathbf{w}; \boldsymbol{\mu}_w^0, \boldsymbol{\Sigma}_w^0)$ is carried out by: (i) adding an attractor for the end position to the linear system, (ii) fixing the starting position, (iii) i.i.d. sampling accelerations to generate trajectories (iv) learning the original ProMP from the sampled trajectories, and finally, (v) conditioning the ProMP on the final joint configuration. The trajectory distributions corresponding to the resulting ProMPs are shown in the top panels of Figure 3. We choose high variance original ProMPs in order to better demonstrate the effect of the constraints. The experiments in Section III-B, however, demonstrate a more balanced interplay between the original ProMPs and the constraints.

In all adaptation problems presented in the following we choose as objective the Kullback-Leibler (KL) divergence either with or without the smoothness regularisation term, as presented in Section II-D2. The smoothness regularisation term consists of a weighted sum of independent regularisations per each joint with joints closer to the base having a higher regularisation weight. For most tasks we used a weighting factor of 0.1 for the overall smoothness regularisation term, while within this term, we used a weighting of [2.0, 0.1, 0.1, 0.1] for the corresponding 4 joints. This weighting reduces the

movement of the first link, which has to move the greatest mass and thus is also the most energy consuming.

We add narrow joint limit constraints for the starting joint angles ($t = 0$) to fix the initial position. In addition to this start-point constraint, we add a waypoint constraint for the end-effector’s Cartesian position $\mathbf{x}_t^{\text{end}}(\mathbf{w})$ at the end of the time interval ($t = T$) to fix the final position the robot has to reach in Cartesian space. In the following we refer to the end-point of the 4th link of the robot as the end-effector. We use location $\bar{\mathbf{x}} = (1.73, 0.0)$ with a radius of $d = 0.05$ for the waypoint constraint at the final time-point. For all constraints in the experiments we choose a confidence level of $\alpha = 0.999$. Each arm link has length 1.0.

All optimisations are carried out using Algorithm 1. The initial value for $\boldsymbol{\theta} = (\boldsymbol{\mu}_w, \boldsymbol{\Sigma}_w)$ is set to $\boldsymbol{\theta}^{s=0} = (\boldsymbol{\mu}_w^0, \boldsymbol{\Sigma}_w^0)$. The initial values for the Lagrange multipliers $\lambda_{k,t}$ corresponding to the start time (initial joint configuration) and end time (end-effector’s Cartesian position) are set to $\lambda_{k,t}^{r=0} = 100$ while the ones corresponding to the rest of the constraint are set to $\lambda_{k,t}^{r=0} = 1.0$.

1) *Waypoint constraints:* We demonstrate the waypoint constraint, by setting a waypoint at location $\bar{\mathbf{x}} = (3.4, 2.0)$ with radius $d = 0.05$ and force the end-effector $\mathbf{x}_t^{\text{end}}(\mathbf{w})$ to stay at that position for one-tenth of the trajectory. Therefore the corresponding constraint is chosen to be active during the time interval $\mathcal{T} = [0.65, 0.75] \subset [0, 1]$. The left-column panels in Figure 3 show the resulting motions’ means and covariances, with 0.95 level sets, for $\mathbf{x}_t^{\text{end}}(\mathbf{w})$ for the KL-

only (middle row) and the KL with smoothness regularised (bottom row) objective, respectively.

When using the KL objective, both the final configuration and generally the overall motion pattern resembles the original ProMP. In contrast when adding the smoothness penalty we obtain a trajectory, which shows clear deviations from the original ProMP. Especially the last part of the trajectory is changed such that the first link moves as little as possible, a behaviour which is incentivised by the smoothness regularisation. Nonetheless the movement stays within the limits created by the original ProMP's confidence bounds.

2) *Repeller constraints*: In this experiment we place a repeller with radius $d = 1.0$ at location $\bar{x} = (2.0, 3.0)$. The end-effector $\mathbf{x}_t^{\text{end}}(\mathbf{w})$ is required to satisfy the repeller constraint during the whole length of the trajectory, hence $\mathcal{T} = [0, 1]$. The second-column panels in Figure 3 show the resulting mean trajectory and the covariances (0.95 level sets) for $\mathbf{x}_t^{\text{end}}(\mathbf{w})$ for the KL-only (middle row) and the smoothness regularised (bottom row) objective, respectively.

The trajectory adaptation resulting from the KL objective can be explained as follows: First, moving the first joint has a large effect on the position of the robot relative to the repelling point, which allows the robot to keep the changes for the rest of the joints minimal compared to the original ProMP. Second, moving further away from the repeller gives the trajectory the possibility to keep a higher variance for the most part of the trajectory. Therefore the KL objective paired with a high variance original ProMP leads to such solutions being favourable. Adding a smoothness regulariser with a proportionally larger weight on the first joint (bottom row) results in a seemingly more natural movement. The latter choice of objective is also plausible in a real environment as the first joint moves more weight and thus consumes more energy.

3) *Non-convex domain constraints*: We place a corner defined by two hyperplanes $\mathbf{n}_1 = (1, 0)$, $\mathbf{b}_1 = (0.5, 0.5)$ and $\mathbf{n}_2 = (0, 1)$, $\mathbf{b}_2 = (0.5, 0.5)$. In this case, we require not only the end-effector $\mathbf{x}_t^{\text{end}}(\mathbf{w})$ to satisfy the constraint, but we also impose the same limitations on the ends of the second and the third link, $\mathbf{x}_t^2(\mathbf{w})$ and $\mathbf{x}_t^3(\mathbf{w})$. The second column from the right in Figure 3 shows the resulting means and covariances (0.95 level sets) for $\mathbf{x}_t^{\text{end}}(\mathbf{w})$ for the KL-only (middle row) and the smoothness regularised (bottom row) objective, respectively.

As expected, the resulting trajectory shows a similar behaviour as in the case of the repeller, however, the configuration of the robot and the non-convex constraint do not allow the robot to keep the final configuration given by the prior. Instead it has to resort to a different motion at this part of the trajectory. Similarly to the repeller experiment, the KL-only objective favours a motion with higher variance, in which the robot can also keep at least part of the trajectory for the last three joints similar to the original ProMP.

4) *Hyperplane constraints*: To demonstrate how a hyperplane constraint affects the motion, we choose a hyperplane with $\mathbf{n} = (1.0, 1.0)$, $\mathbf{b} = (0, 2)$ and we require the end-effector $\mathbf{x}_t^{\text{end}}(\mathbf{w})$ and the penultimate joint $\mathbf{x}_t^3(\mathbf{w})$ to satisfy it. Similar to the experiment with non-convex domains, in

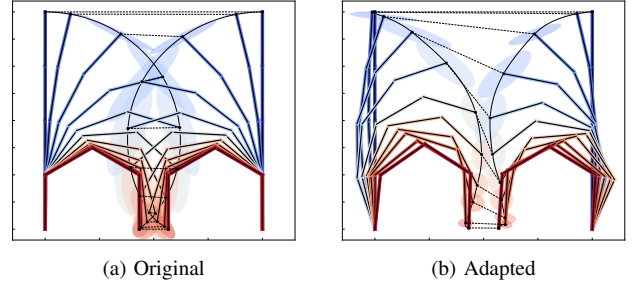


Fig. 4. *Illustrating mutual avoidance for two planar robots*. In this figure we show the results of the mutual avoidance experiment in Section III-A5. The left panel shows the independently learned original ProMPs, the right panel shows the combined ProMP, adapted with the mutual avoidance constraint from Section II-E5. Analogous to Figure 3, the colour gradients show time progression and the shaded ellipses stand for the end-point's covariances. Mutual avoidance is realised by the left robot slowing down and the right robot speeding up its motion.

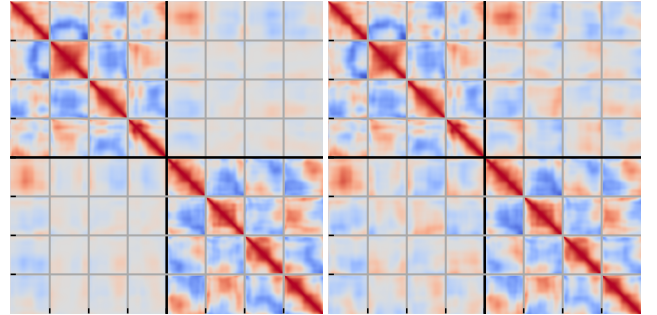


Fig. 5. *Illustrating the choice of objective for the mutual avoidance problem*. The panels show the correlations in the adapted joint trajectories when using the objectives $D_{\text{KL}}[p(\mathbf{w}_1, \mathbf{w}_2) \| p_0(\mathbf{w}_1) p_0(\mathbf{w}_2)]$ (left panel) and $D_{\text{KL}}[p(\mathbf{w}_1) \| p_0(\mathbf{w}_1)] + D_{\text{KL}}[p(\mathbf{w}_2) \| p_0(\mathbf{w}_2)]$ (right panel). The colour indicates the correlation from -1 (blue) through 0 (grey) to +1 (red). The small blocks stand for the robot's joints, whereas the large ones stand for the two robots. As expected, the covariance agnostic objective leads to higher correlations between the robots.

this setup the movement and the final configuration have to be significantly different to that of the original ProMP. The right-column panels in Figure 3 show the resulting means and covariances, with 0.95 level sets, for $\mathbf{x}_t^{\text{end}}(\mathbf{w})$ for the KL-only objective (middle row) and the weighted sum with smoothness regularisation (bottom row), respectively. Note that the original ProMP is depicted in the top right panel, where the original movement mainly has a different start configuration and a higher variance.

We observe that the adapted primitive results in a movement similar to the experiments with the repeller and the non-convex constraint. The robot first moves away from the constraint boundary in order to take a configuration that makes the final objective easier to reach. As we have seen in the two previous cases, the KL-only objective produces a high variance trajectory, whereas the smoothness regularisation leads to a reduced variance and more a direct approach towards the target end-point. Note that modelling the primitive in joint space allows us to force not only the end-effector, but also the whole robot arm to stay inside the domain defined by the hyperplane.

5) *Mutual avoidance constraints*: Besides illustrating the mutual avoidance constraint, in this experiment we investigate the effect of the two different options for choosing the KL objective, as described in Section II-E5. We designed a dual-arm setting with two planar robot arms, which are placed in the configurations shown in Figure 4. This configuration would lead to a collision should the trajectories be executed simultaneously. The corresponding original ProMPs are learnt independently. We set one mutual avoidance constraint for the end-effectors, namely, $P_w(|\mathbf{x}_t^{1,\text{end}}(\mathbf{w}) - \mathbf{x}_t^{2,\text{end}}(\mathbf{w})|^2 > d_{\text{end}}^2) \geq \alpha$ and two constraints for the end-effectors and the last joints $P_w(|\mathbf{x}_t^{1,4}(\mathbf{w}) - \mathbf{x}_t^{2,\text{end}}(\mathbf{w})|^2 > d_c^2) \geq \alpha$ and $P_w(|\mathbf{x}_t^{1,\text{end}}(\mathbf{w}) - \mathbf{x}_t^{2,4}(\mathbf{w})|^2 > d_c^2) \geq \alpha$, respectively. We use $d_{\text{end}} = 0.4$ and $d_c = 0.8$ for the corresponding distances. We then adapt an extended joint model with weights $\mathbf{w} = (\mathbf{w}_1, \mathbf{w}_2)$, see Section II-E for details. The original ProMP and the adapted ProMP are shown in Figure 4.

We observe that the collision is avoided by a speed-up of the right-robot and a slow-down of the left-robot’s motion, when compared to the original ProMPs. The motion pattern and the final configurations, however, remain similar. The optimisation problem has two modes, either the left or the right robot speeds up its motion. Depending on the trajectories sampled to learn the two original ProMPs, the optimisation chooses one of the two modes. Indeed, we observed a correlation between small fluctuations in the original ProMPs and the choice of mode in the optimisation.

When comparing the two objectives we propose in Section II-E, we were particularly interested in the effect they have on the learnt correlations between the motion of the two robots. In Figure 5 we show the correlation corresponding to the joint space coordinates of the two robot arms. While both objectives result in trajectory samples with no collisions, $D_{\text{KL}}[p(\mathbf{w}_1, \mathbf{w}_2) \| p_0(\mathbf{w}_1)p_0(\mathbf{w}_2)]$ (left panel) tends to penalise high correlation. Note that the learned correlations between links or between robots can encode useful task specific information, as is shown in Section III-C4.

In this section we carried out a series of experiments to show how our trajectory adaptation method works in a simulated environment. We designed tasks that shed light on how each constraint introduced in Section II-E can be used and showed how the different weightings of the Kullback-Leibler divergence—similarity to the original ProMP—and the smoothness regularisation term affect the resulting trajectories. In the next section these results are validated with real robot arms.

B. Avoidance Adaptation for a Real Robot

To demonstrate how our proposed adaptation method works in a real environment, we used two Franka Emika 7-DoF robot arms. We designed several experiments starting with simple avoidance problems such as the repeller and the hyperplane in this section and continuing with two mutual avoidance problems in dual-arm settings in the next two Sections. The Cartesian coordinates we reference are relative to the robot’s base, with the x -axis pointing forward; distances are measured

in meters. In the dual arm settings we use the coordinate system of the robot on the left in Figure 8.

The sample trajectories used to learn the original ProMP $\mathcal{N}(\mathbf{w}; \boldsymbol{\mu}_w^0, \boldsymbol{\Sigma}_w^0)$ are recorded by moving the robot arm through the trajectories by hand as illustrated in the supplementary video. In all experiments, we record the joint space coordinates of the robot(s). To execute trajectories we use a joint space PD controller in the following way: (i) we sample a weight vector $\bar{\mathbf{w}}$ from the distribution of interest, be it either $\mathcal{N}(\mathbf{w}; \boldsymbol{\mu}_w^0, \boldsymbol{\Sigma}_w^0)$ or $\mathcal{N}(\mathbf{w}; \boldsymbol{\mu}_w, \boldsymbol{\Sigma}_w)$ (ii) we evaluate the (joint space) trajectory $\mathbf{z}_t(\bar{\mathbf{w}})$ at 101 equidistant time-points (iii) we use piecewise linear interpolation with time as the running variable and follow the trajectory with the PD controller.

1) *Obstacle avoidance with repeller and hyperplane constraints*: In this experiment we designed two simple avoidance problems to test the repeller and hyperplane constraints, respectively. First, we learn a ProMP to move the robot’s end-effector across the table to a target object. Then we adapt it to avoid a ball on the table and a stack of books as shown in Figure 7a. For the former we use a repeller constraint while for the latter we use a hyperplane constraint. We record the sample trajectories by moving the end-effector from a random position within the larger area, marked by tape on the left side of the table, to a suitable position for grasping the grey cube. We use a variety of starting positions and explore several modalities such as moving the arm diagonally close to the surface of the table, around, both close to the base and far away from it, and diagonally in an arch above the table. In both adaptation problems we use an additional hyperplane constraint that forces the end-effector to stay 0.01m above the surface of the table.

In the first experiment we place a repeller with radius $d = 0.1$ at location $\bar{\mathbf{x}} = (0.5, 0, 0.1)$. The resulting adapted paths are visualised in Figure 6b and the execution of samples can be seen in the video in the Supplementary Material. As we can observe in Figures 6b and the corresponding video, the adaptation method still preserves a lot of variability, leaving out only the trajectories that move diagonally close to the surface of the table. In particular, the sample paths on Figure 7a show that the adapted ProMP still encodes trajectories that move above (top row) and around (middle row) the repeller represented by the ball. The red marginal means and ± 3 standard deviations in Figure 7b show that adaptation shifted the mean trajectory upward and removed a significant proportion of the variability along the z -axis. The marginal probability mass still left below the 0.2m height of the repeller accounts for the trajectories that move around the ball. A comparison with the hyperplane constraint, which is discussed below and plotted in green, shows that the shift upwards is not solely due to the hyperplane constraint representing the surface of the table, but also to the removal of the above mentioned modality.

In the second experiment we place a hyperplane at $\mathbf{b} = (0.4, 0, 0)$ with $\mathbf{n} = (1, 0, 0)$ to restrict the robot’s workspace. The adaptation restricts the trajectories to lie behind the hyperplane thus keeping only the trajectories that reach across the table by moving the end-effector close to the robot’s base as shown in the bottom row of Figure 7a. The top panel (x -

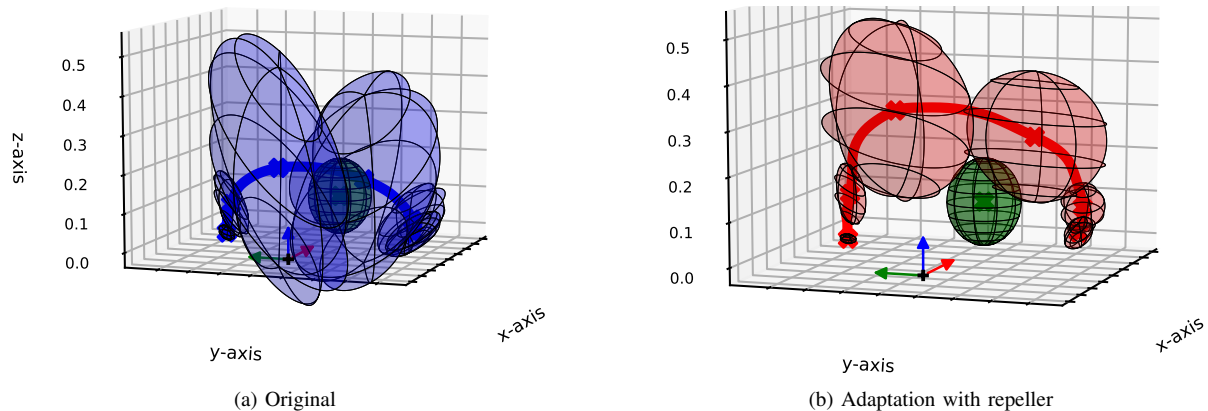


Fig. 6. In this Figure we show the end-effector’s Cartesian trajectory before and after adaptation with a repeller. The thick lines indicate the mean, while the ellipsoids depict the 0.95 level sets at several locations. The green sphere represent the constraint location and margin. The Figure on the left shows the original trajectory after encoding the demonstrations, whereas the Figure on the right shows the trajectory distribution after adaptation.

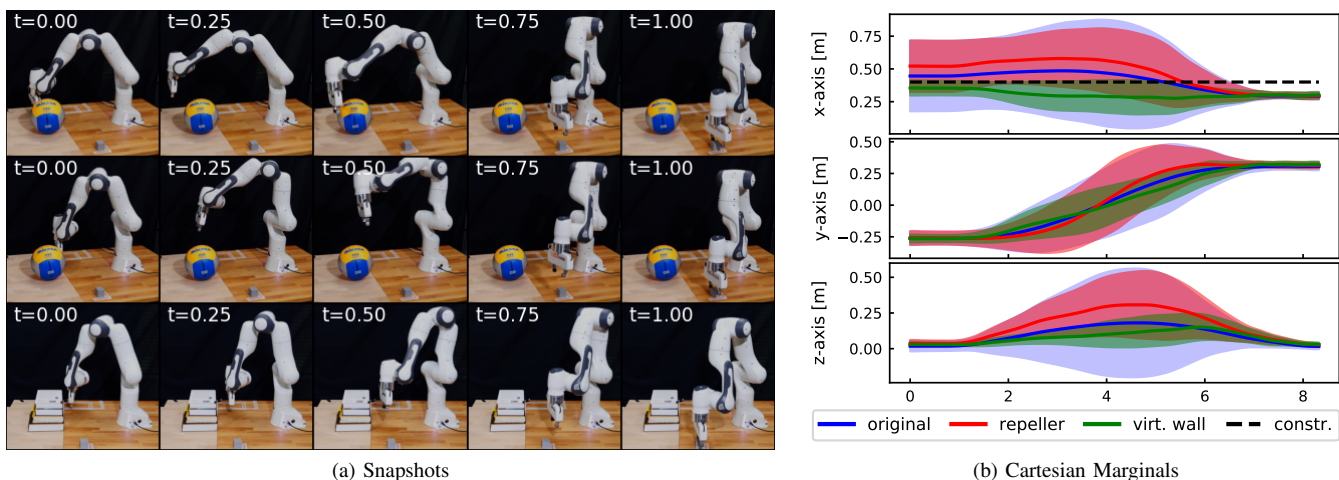


Fig. 7. *Illustrating Cartesian constraints on a real robot.* Figure 7a shows samples from the primitive adapted with the repeller (top two rows) and the hyperplane (bottom row). We can see the adapted ProMPs capture multiple of the demonstrated modes, this is especially visible the first half of the trajectories. The marginal distribution of the the end-effector trajectories in Cartesian space is displayed in Figure 7b with means and ± 3 standard deviations. Both adaptations remove the probability mass corresponding to trajectories below the table (at $z = 0$) and the hyperplane constraint (virt. wall) additionally does not include trajectories far from the robot’s base (large x values).

axis) in Figure 7b highlights that adaptation indeed removed all probability mass outside the half space defined by the hyperplane. We emphasise that in both of these experiment we used neither start- nor end-constraints. The robot has been conveniently trained from demonstrations and the original ProMP encoded the important parts of the reaching task in the variance. Staying close to the original ProMP allows us to reach a suitable grasping position at the end of each trajectory.

C. Mutual avoidance in a dual-arm setting

In this set of Experiments we demonstrate a range of constraints from our adaptation framework in a dual arm setting. First, we show that the mutual avoidance constraint can be used to combine two robots with individually learned ProMPs in the same workspace. Second, we use the joint limit constraints to fix a known problem of ProMPs. Third, we investigate the effect of the smoothness regularisation in a real robot setting. Finally, we examine the cross correlations of the

combined primitive and we show that the adaptation encodes task-specific knowledge into the primitive. In all experiments we use two Franka Emika Panda robots with their bases $1.13m$ apart, facing each other, as shown in Figure 8. The original task for both robots is a reaching motion, in which the end-effector has to move from the robot’s left to it’s right as indicated by the arrows in Figure 8. We independently demonstrate and learn separate ProMPs for each robot arm and then use our method to obtain a combined primitive with simultaneously executed, collision-free trajectories.

1) *Combining primitives in the same workspace:* For reasons of clarity we explicitly state the adaptation problem in mathematical form. Let $p_0(w_1)$ and $p_0(w_2)$ be the two independently learned ProMPs and let $p(w)$ with $w = (w_1, w_2)$ denote the (jointly) adapted ProMP. In order to define constraints for collision avoidance, we choose three points of interest on each robot $x_t^{1:1:3}(w_1)$, and $x_t^{2:1:3}(w_2)$, respectively. The placement of the points of interest and the

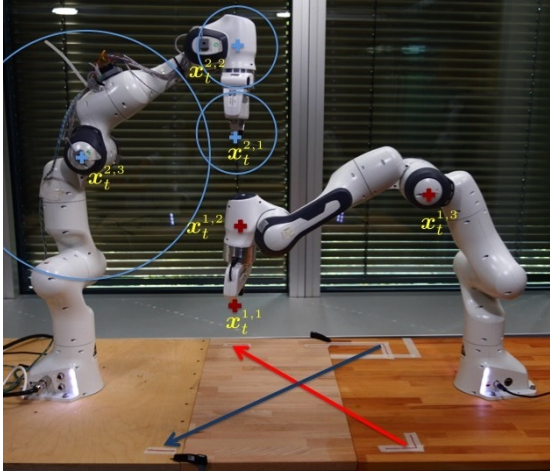


Fig. 8. This Figure shows the experimental setting of the experiments described in Section III-C. The arrows display the directions of motion for the left (blue) and right (red) robot, respectively. The red and blue crosses display the points of interest used for the mutual avoidance constraints and the circles show the corresponding margins.

distances corresponding to the mutual avoidance constraints are shown in Figure 8. One could add avoidance constraints for all possible collisions for the chosen points of interest, however, the number of constraints does not necessarily have to grow quadratically with the number of points of interest because in many practical applications a large proportion of collisions are physically improbable. Therefore, we choose 5 of the possible 9 constraints, these are specified by the index pairs and their corresponding distance $(i, j, d_{ij}) \in \mathcal{G} = \{(1, 2, 0.1), (2, 1, 0.1), (2, 2, 0.1), (2, 3, 0.3), (3, 2, 0.3)\}$. Additionally, we use a hyperplane constraint with parameters $\mathbf{n} = (0, 0, -1), b = (0, 0, 0.01)$ to keep the end-effectors above the surface of the table.

Given these assumptions, we formulate the resulting adaptation problem as

$$\begin{aligned} \min_p \quad & D_{\text{KL}}[p(\mathbf{w}) \| p_0(\mathbf{w}_1) p_0(\mathbf{w}_2)] \\ \text{s.t.} \quad & P_w(|\mathbf{x}_t^{1,i}(\mathbf{w}_1) - \mathbf{x}_t^{2,j}(\mathbf{w}_2)|^2 > d_{ij}^2) \geq \alpha_c, \quad (i, j, d_{ij}) \in \mathcal{G} \\ & P_w(\mathbf{n}^T(\mathbf{x}_t^{i,1}(\mathbf{w}_i) - \mathbf{b}) \leq 0) \geq \alpha_{\text{hp}}, \quad i = 1, 2 \end{aligned} \quad (24)$$

where we set $\alpha_c = \alpha_{\text{hp}} = 0.999$. Optimisation is carried out with Algorithm 1.

The mean trajectories of the original ProMP are plotted in Figure 9 showing that the end-effectors would collide if the trajectories were executed simultaneously. The adaptation has a stronger effect on the motion of the left robot resulting in trajectories that move the end-effector on top of the right robot. Additionally, the adaptation shapes both trajectories in a way that increases the distance between both robots. The video in the Supplementary Material shows several samples from the adapted primitive.

This experiment also shows the distinct advantage of probabilistic approaches for primitives over their deterministic counterparts. The probabilistic approach allows the adaptation to have a stronger effect on parts of the trajectory that have a larger variance and thus are less essential for the reaching

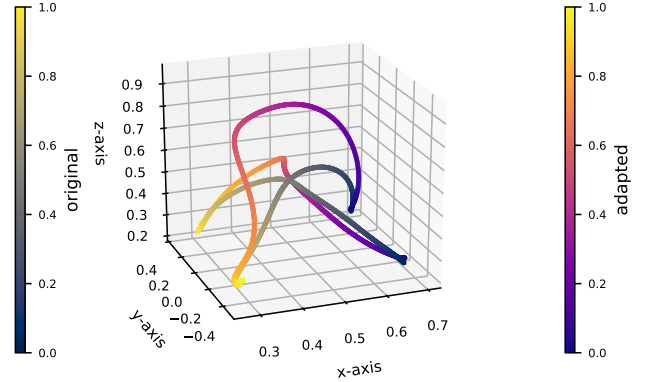


Fig. 9. In this Figure we show the mean trajectories of the points of interest $x_t^{1,2}$ and $x_t^{2,2}$ (see Figure 8) before (original) and after adaptation. Time is indicated by the colour gradients. If executed the original primitives would lead to a collision of the robots, whereas the adaptation shapes the trajectories to be collision-free.

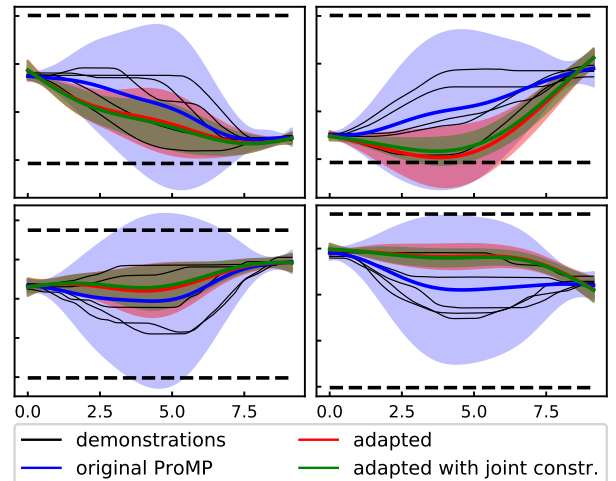
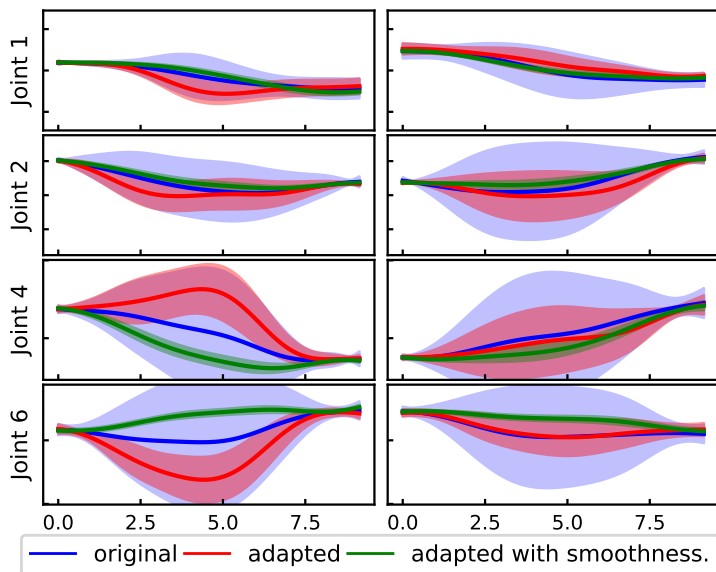


Fig. 10. We visualise the trajectories of joints 4 and 6 in experiment III-C2. We show the demonstrations (black) and the mean with ± 3 standard deviations of the primitive before (blue) and after adaptation (red and green). Solving the adaptation problem described in eq. (24) results in the primitive shown in red, whereas the primitive shown in green uses additional limit constraints at the joint limits (dashed black). Even though all demonstrations stay within the joint limits, both the original ProMP and the ProMP adapted without limit constraints can have mass outside of the feasible limit.

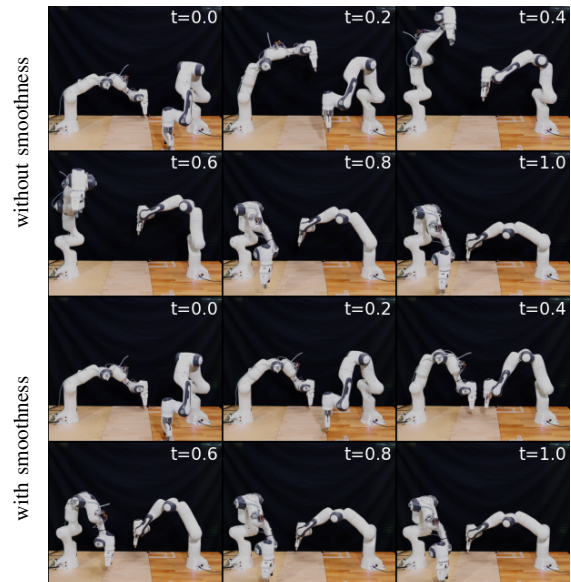
task. In the following we introduce various modifications to the this mutual avoidance experiment in order to examine specific details of our method.

2) *Respecting joint limits*: A side-effect of modelling with ProMPs is that even though all demonstrated movements stay within the robot's joint limits, the ProMP can have mass outside of the limits. Accordingly, we can apply the joint space constraints to prevent joints going off-limits in the adapted ProMP. In Figure 10 we visualise the application of limiting the ProMP in joint space directly, as described in Section II-D1. Observe how adaptation with additional joint limits, shown on green, removes joint limit violations when compared to the original (blue) and adapted (red) ProMPs.

3) *The effect of Smoothness Regularisation*: We compare adaptation with and without smoothness regularisation by



(a) Smoothness Regularisation: Joint Space marginal distribution



(b) Smoothness Regularisation: Snapshots

Fig. 11. This Figure demonstrates the effect of smoothness regularisation. On the left we visualise the joint space marginals with mean and ± 3 standard deviations. We compare the original ProMP (blue) to the ones adapted with (green) and without (red) smoothness regularisation. The right Figure shows snapshots of the mean trajectories, with (bottom two rows) and without (top two rows) smoothness, executed on the robots. We can see that the smoothness regularisation significantly reduces the remaining variance and results in a smoother trajectory. Instead of moving the left robot on top of the right one, the smooth trajectories use the available space between the two robots by moving both of them closer to their own bases.

adding a regularisation term $\kappa E_{p(w)}[R(w)]$ with $\kappa = 0.1$ to (24) without any additional joint weighting. Figure 11a shows the marginal trajectories for a few relevant joints while Figure 11b compares snapshots of the resulting mean trajectories. We can observe that smoothness regularisation reduces the variance and results in a significantly different trajectory distribution. Similarly to the toy example in Figure 1, the adapted trajectory exhausts the margins given by the constraints to maximise smoothness. This is particularly evident when comparing the trajectories visualised in Figure 11b: instead of moving one robot on top of the other, the mean trajectory shown in the bottom two rows barely keeps the enforced distance but is much more economical. The video in the Supplementary Material shows the different trajectories executed side-by-side for a better comparison.

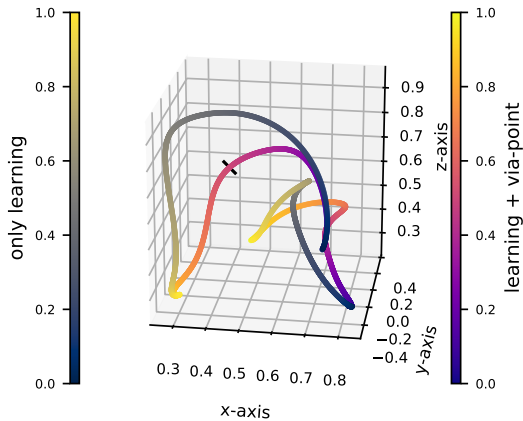
4) *Adaptation encodes task specific knowledge*: An important advantage of the probabilistic approach is that it can capture covariances of the robot’s motion. These covariances exist not only between individual joints of the same robot, but they also link the joints of different robots. This implies that task specific knowledge, like the robots avoiding each other, can be encoded in the covariance matrix Σ_w . To test this hypothesis we designed the following experiment: we condition the adapted ProMP, using the KL-only objective from Section III-C1, on a via-point in the joint space of the left robot to measure the effect it has on the right robot’s trajectories. We place the via-point in the joint space and force the left robot to move through the Cartesian position shown in Figure 12a. At the same time we observe the change of course from the right robot. In this experiment we use the sum of marginal KL’s objective $D_{\text{KL}}[p(w_1)||p_0(w_1)] + D_{\text{KL}}[p(w_2)||p_0(w_2)]$ (see

Sections II-E5 and III-A5), to incentivise stronger correlations between the two robots. The via-point conditioning results in the left robot’s trajectory moving closer to the right robot, both in x and z direction, as is shown in Figure 12b. Furthermore, the figure shows the right robot adapting its trajectory accordingly, by moving closer to the table and further away from the left robot’s base. We can observe that, as expected, the right robot’s trajectory has changed in a suitable way to reduce the likelihood of a collision, thus correlations in the adapted ProMP do indeed encode avoidance to a measurable degree. Note, however, that by conditioning only we do not obtain guaranteed collision avoidance since avoidance is not enforced by a constraint. We also want to emphasise that this task specific knowledge must have been added during the task specific adaptation with constraints, as the original ProMP was learned from individual motions. The video in the Supplementary Material also visualises this experiment and shows an image of the ProMP correlations before and after adaptation.

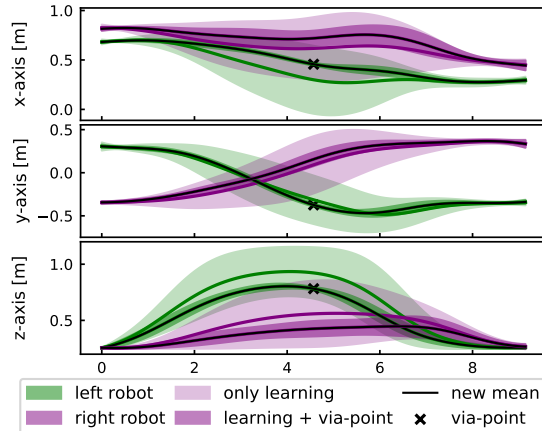
In this set of experiments we showed how joint adaptation of ProMPs can be carried out in a real world scenario. This type of adaptation can be useful in many practical applications where several robots, each having their own independently trained tasks, can be adapted and reconfigured to operate in the same environment. We also showed that the adaptation process can add task specific knowledge to the ProMP, making downstream adaptations, like conditioning, have a more informed effect.

D. Mutual avoidance with unbound waypoints

In the previous experiment we showed how to combine multiple individual primitives into a combined motion, allowing us



(a) Via-point conditioning: 3D overview



(b) Via-point conditioning: Cartesian marginal distribution

Fig. 12. This Figure accompanies the experiment on encoding task specific knowledge during adaptation, which is described in Section III-C4. The left Figure shows the mean Cartesian trajectories of the points $x_t^{1,2}$ and $x_t^{2,2}$ (see Figure 8) on both robots once after adaptation (only learning) and once after we conditioned the adapted ProMP on a via-point (learning + via-point). Time is indicated by the colour gradients and the black "x" in both images represents the joint space via-point transformed through the forward kinematics. Figure 12b shows the corresponding Cartesian marginal distributions, also before (low alpha) and after (high alpha) conditioning. We can clearly see that conditioning the left robot also significant changes the trajectory of the right robot, that is the right robot moves further away from the path of the left robot.

to reconfigure robots in close proximity. However, the adaptation could find collision-free trajectories by just coordinating the robots spatially, because the key points both robots had to visit—the start and end location of their motions—were naturally distinct for both robots. In manufacturing tasks this setup can be violated because multiple robots might have to visit the same location requiring not only spatial, but also temporal coordination. Inspired by a pick-and place task, in which two robots have to grasp objects out of the same box, we designed an experiment where we require the two robots end-effectors $x_t^1(\mathbf{w}_i)$ and $x_t^2(\mathbf{w}_i)$ to visit the same location in Cartesian space without colliding. Compared to the previous adaptation, this is a somewhat more challenging problem requiring us to specify the task relevant parameters with constraints of the form: visit a specific location at least once during the trajectory while staying away from the other robot all the time. This task requires us to combine collision avoidance with temporally unbound waypoints, described in Section II-E. To demonstrate this adaptation task we used the dual arm setup shown in Figure 13b. The robots are placed next to each other with parallel x -axes and are required to perform a round-trip trajectory to the middle of the table. Similarly to the experiment presented in the previous section, we demonstrate and learn two independent ProMPs $p_0(\mathbf{w}_1)$ and $p_0(\mathbf{w}_2)$ and then adapt them jointly.

To formulate the adaptation problem, we use the following constraints for the end-effectors $x_t^1(\mathbf{w}_1)$ and $x_t^2(\mathbf{w}_2)$: (i) a mutual avoidance constraint; (ii) temporally unbound waypoints for both end-effectors at location \bar{x}_{middle} ; (iii) waypoint constraints for the start and end locations \bar{x}_0^i and \bar{x}_T^i ; (iv) a hyperplane constraint to keep both end-effectors above the surface of the table. By using a similar notation like in the previous section, the adaptation problem is formalised as

$$\min_p D_{\text{KL}}[p(\mathbf{w}) \| p_0(\mathbf{w}_1) p_0(\mathbf{w}_2)] + \kappa E_{p(\mathbf{w})}[R(\mathbf{w})] \quad (25)$$

$$\begin{aligned} \text{s.t. } & P_{\mathbf{w}}(|\mathbf{x}_t^1(\mathbf{w}_1) - \mathbf{x}_t^2(\mathbf{w}_2)|^2 > d_{\text{coll}}^2) \geq \alpha_{\text{coll}} \\ & \max_t P_{\mathbf{w}}(|\mathbf{x}_t^i(\mathbf{w}_i) - \bar{\mathbf{x}}_{\text{middle}}|^2 \leq d_{\text{middle}}^2) \geq \alpha_{\text{middle}} \\ & P_{\mathbf{w}}(|\mathbf{x}_{t=0}^i(\mathbf{w}_i) - \bar{\mathbf{x}}_0^i|^2 \leq d_{i,0}^2) \geq \alpha_0 \\ & P_{\mathbf{w}}(|\mathbf{x}_{t=T}^i(\mathbf{w}_i) - \bar{\mathbf{x}}_T^i|^2 \leq d_{i,T}^2) \geq \alpha_T \\ & P_{\mathbf{w}}(\mathbf{n}^T(\mathbf{x}_t^i(\mathbf{w}_i) - \mathbf{b}) \leq 0) \geq \alpha_{\text{hp}}, \quad i = 1, 2. \end{aligned}$$

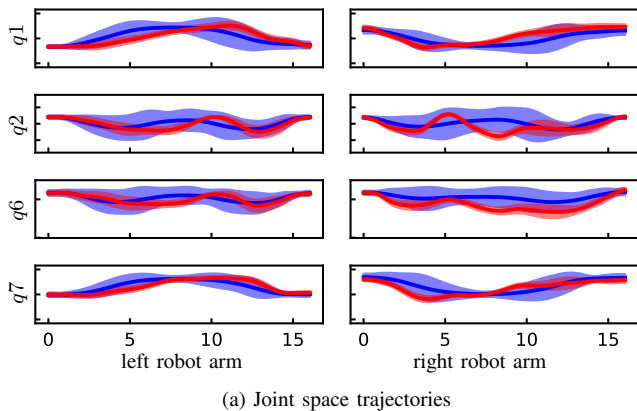
We set α_{coll} , α_{middle} , α_0 , α_T and α_{hp} to 0.999 and use Algorithm 1 to solve the optimisation problem. The resulting adapted ProMP is illustrated in Figure 13 and supplementary Video. Since both end-effectors have to visit $\bar{\mathbf{x}}_{\text{middle}}$, collision avoidance happens through the left arm delaying and the right arm speeding up its motion towards $\bar{\mathbf{x}}_{\text{middle}}$. As we can observe in Figure 13a, the left arm moves slowly during the first part of the trajectory followed by fast movement during the second part. The right arm displays a complementary motion pattern.

While in the previous example the constraint allowed a large variety of trajectories without collision, in this example, avoiding collision requires a much finer temporal coordination. We believe that this is due to the strict geometric constraints and the temporal dependencies prompted by the unbound waypoint.

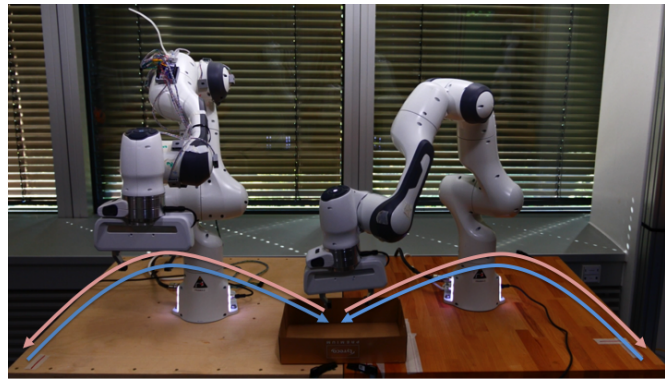
In this experiment we demonstrated that highly non-trivial path constraints such as the unbound waypoint can be implemented by the proposed adaptation method. This constraint can be further generalised by requiring the arm to spend a certain amount of time at the unbound waypoint. We can then use this time to perform some additional task which is not necessarily part of the ProMP, say, a pick or drop task.

IV. RELATED WORK

Adapting movement primitives to new scenarios is a central element in every primitive framework. In this section we



(a) Joint space trajectories



(b) Experimental setup.

Fig. 13. Illustrating a mutual avoidance task with unbound waypoints. The panel (b) illustrates the experimental setup for the mutual avoidance task presented in Section III-D. The arrows show the first (blue) and second (red) parts of the original ProMP trajectories together with a snapshot of the adapted trajectories (background). Figure (a) shows the relevant joint space trajectories, joints 1, 2, 6 and 7, of both robots. The original and adapted ProMPs are shown in blue and red, respectively. Adaptation results in the left arm delaying (see flat sections in the first half of the trajectory) and the right arm speeding up its movement towards the middle.

discuss the related work on primitive adaptation and we draw connections to our own approach.

DMPs formulate primitives in terms of dynamic systems, which allows a convenient extension to obstacle avoidance by adding repellent points to the spring-damper behaviour [6]. This concept has been extended to multiple obstacles [7], non-point obstacles [8] and the authors of [9] proposed an online model predictive controller based on DMPs for tackling online obstacle avoidance. In our approach we also presented repellent points as one way to achieve obstacle avoidance. Specifically, the direct probabilistic encoding of trajectories allows us to formulate repellers in terms of excluding a specific region in space from the primitive. This has the advantage that we can explicitly specify a margin instead of tuning the repellent force. Furthermore, we can exploit the unscented transform to add repellent points to any point of interest on the robot.

Another extension of the DMP framework incorporates joint limits [10]. This extension is based on transforming the DMP into a space in which the joint limits correspond to $\pm\infty$ [33]. In Section II-D1 we discussed how ProMPs could use the same technique for joint limit avoidance. Besides joint limits, our method can also operate with time varying limits and demonstrations that do not fulfil the limits in the first place. In [11], the authors modified the dynamic system governing the DMP’s evolution of time to guarantee staying within velocity limits without perturbing the trajectory. In our approach joint velocity limits could be handled with the limit constraints presented in Section II-D1, however, one has to encode the joint velocity directly in the ProMP. Moreover, limits on Cartesian velocity could be handled analogously to hyperplane constraints, relying on the robot’s Jacobian to transform the ProMP linearly into Cartesian velocity space. Finally, the combination of multiple DMPs has been studied in [34]. Similar to our approach, the authors use constrained optimization, in their case to incorporate the robot’s equations of motion. However, in theory their formulation allows constraints on joint torques, joint acceleration and wrench forces.

The GMM-GMR framework can formulate adaptation by combining multiple primitives, representing different skills, into one. In [13] the authors combines task space and joint space primitives. The author uses linear, Jacobian-based transformations to map different primitives into the same space in which they are merged using Gaussian multiplication. Combination through Gaussian multiplication is the basis for a range of adaptation techniques in the framework: Task parametrized Gaussian mixture models (TP-GMM) [14] use different linear transformations to record the same primitive from different frames. After learning, adaptation can be done by changing the transformation function to generalise a primitive to, for example, unseen start- or end-points. In [35] TP-GMM is extended to include frames representing Cartesian orientation and the authors apply their method to a bimanual setting. The same authors develop an approach for combining primitives based on learned task hierarchies in [16]. Similar to our method, the aforementioned approaches allow adaptation in both joint and task-space. In Section II-F we sketched how a combination of primitives could be performed in our framework, however, the main focus of our paper lies on using constraints to formulate adaptation in terms of including and excluding behaviour from learned primitives.

In [15] the authors formulate the combination of multiple ProMPs based on Gaussian multiplication. In the same work, the author tackles obstacle avoidance by adding a primitive which explicitly moves around an added obstacle. In our framework obstacle avoidance is best handled with a repellent point, however, the combination of different ProMPs based on Gaussian multiplication could be used before or after adaptation to exploit the redundancy of a manipulator and solve multiple tasks in parallel.

A different approach to obstacle avoidance, based on trajectory optimization with repellent points, has been presented in [17]. The trajectory distribution is modelled as a Gaussian on a discretisation of the Cartesian path. This distribution is optimised to stay as close as possible to a given ProMP—also in the Cartesian space—while maximising a reward function

which incentivises obstacle avoidance. After optimisation, samples from the trajectory distribution are used to learn a new (adapted) Cartesian space ProMP. This ProMP is then subsequently used for online via-point conditioning as presented in [3]. In comparison, our approach can be used with ProMPs which directly parametrise joint space trajectories and we formulate obstacle avoidance as constraints thus removing the need for tuning a reward function. Additionally, we can achieve obstacle avoidance for multiple robot links, by using the unscented transform combined with the robot’s forward kinematics.

In [18], [19] the authors use ProMPs as a basis for online obstacle avoidance. They formulate a deterministic approach to obstacle avoidance by minimising the Mahalanobis distance to the original ProMP, while at the same time keeping a defined distance to an obstacle. This has the benefit of requiring fewer parameters, making the method realtime feasible. However, having a distribution over trajectories allows us to learn useful correlations, between individual joints as well as between different robots, allowing improved adaptation afterwards, as we showed in Section III-C4. In general, our approach can be used to pre-adapt a given ProMP to new situations, with online obstacle avoidance as described in [18], [19] being used afterwards to react to dynamically changing conditions.

In [21] and in a follow-up work [22] the authors show how to adaptively condition a ProMP learned in joint space on a desired end-effector position, orientation and velocity. They present a table-tennis task where the robot’s striking motion has to be dynamically conditioned on the predicted hitting point of a moving ball. The approach relies on a first order expansion of the robot’s forward kinematics and uses a Laplace approximation to find a Gaussian posterior for conditioning. This is a particularly well suited method for fast real-time adaptation with Cartesian via-points, it can also be used in combination with a ProMP adapted by our method.

V. CONCLUSIONS

In this paper we introduce a probabilistic framework for adapting Probabilistic Movement Primitives to new scenarios. ProMPs can be conveniently learned from demonstrations and they encode relevant information about a important points of the task in their variance. We formulate adaptation as a constrained optimisation problem where we constrain the probability mass associated with undesired trajectories to be low. We derive a variety of constraints that can be used as tools to shape the distribution over trajectories both in joint and task space. This enables us to formulate and solve a rich class of adaptation problems such as: joint limiting, virtual walls in Cartesian coordinates, obstacle avoidance, and mutual avoidance of several robots.

There are several important immediate practical applications of our approach. In Section II-D2 we introduce smoothness regularisation that can be used as an ad-hoc tool for regularisation when one is agnostic about the number of basis functions in the ProMP. The resulting smooth trajectories are also easier to control. In Section III-C we show how the inherent problem of ProMPs in modelling bounded joints with

unbounded Gaussian variables can be addressed and partially rectified by using joint limiting constraints. Having virtual walls is an important requisite for the safe operation of robots in confined workspaces. In the experiments in Section III-B1 we show how virtual walls can be implemented in a real world environment. The mutual avoidance adaptation presented in Sections III-C and III-D show how our framework can be successfully applied to reconfigure robots with independently learnt tasks to jointly operate in the same workspace.

Retaining a full probabilistic approach in adaptation comes with the disadvantage of having a large number of parameters—a quadratic number of parameters when compared to the deterministic approaches. This makes the numerical optimisation too slow to operate in a real time fashion, however, previously presented approaches for online avoidance can be used after adapting a primitive with our framework. Additionally, we showed in Section III-C4 how post-optimisation adaptations can have a more informed effect, due to the addition of task specific knowledge to the primitive.

We also foresee several options for speeding up optimisation and deriving an online adaptation framework. For example, one can consider reducing the number of covariance parameters (e.g. sparse structures), reducing the number of effective parameters by using limited time windows for adaptation, and using first order expansions instead of the unscented transform.

ACKNOWLEDGMENT

The authors would like to thank their colleagues at the Volkswagen Group Machine Learning Research Lab for their valuable suggestions towards improving the manuscript and for their contributions to the robotics setup used in this work.

REFERENCES

- [1] A. J. Ijspeert, J. Nakanishi, and S. Schaal, “Learning Attractor Landscapes for Learning Motor Primitives,” in *Advances in Neural Information Processing Systems 15*. MIT Press, 2003, pp. 1547–1554.
- [2] A. J. Ijspeert, J. Nakanishi *et al.*, “Dynamical Movement Primitives: Learning Attractor Models for Motor Behaviors,” *Neural Computation*, vol. 25, no. 2, pp. 328–373, Nov. 2012.
- [3] A. Paraschos, C. Daniel *et al.*, “Probabilistic Movement Primitives,” in *Advances in Neural Information Processing Systems 26*. Curran Associates, Inc., 2013, pp. 2616–2624.
- [4] S. Calinon, F. Guenter, and A. Billard, “On Learning, Representing, and Generalizing a Task in a Humanoid Robot,” *IEEE Transactions on Systems, Man, and Cybernetics, Part B (Cybernetics)*, vol. 37, no. 2, pp. 286–298, Apr. 2007.
- [5] S. Chiappa, J. Kober, and J. R. Peters, “Using Bayesian Dynamical Systems for Motion Template Libraries,” in *Advances in Neural Information Processing Systems 21*. Curran Associates, Inc., 2009, pp. 297–304.
- [6] D.-H. Park, H. Hoffmann *et al.*, “Movement reproduction and obstacle avoidance with dynamic movement primitives and potential fields,” in *IEEE-RAS International Conference on Humanoid Robots*, Dec. 2008, pp. 91–98.
- [7] H. Hoffmann, P. Pastor *et al.*, “Biologically-inspired dynamical systems for movement generation: Automatic real-time goal adaptation and obstacle avoidance,” in *IEEE International Conference on Robotics and Automation*, May 2009, pp. 2587–2592.
- [8] M. Chi, Y. Yao *et al.*, “Learning, Generalization, and Obstacle Avoidance with Dynamic Movement Primitives and Dynamic Potential Fields,” *Applied Sciences*, vol. 9, no. 8, p. 1535, Jan. 2019.
- [9] R. Krug and D. Dimitrov, “Model Predictive Motion Control based on Generalized Dynamical Movement Primitives,” *Journal of Intelligent & Robotic Systems*, vol. 77, no. 1, pp. 17–35, Jan. 2015.
- [10] A. Duan, R. Camoriano *et al.*, “Constrained DMPs for Feasible Skill Learning on Humanoid Robots,” in *IEEE-RAS International Conference on Humanoid Robots*, Nov. 2018, pp. 1–6.

- [11] A. Dahlin and Y. Karayiannidis, "Adaptive Trajectory Generation Under Velocity Constraints Using Dynamical Movement Primitives," *IEEE Control Systems Letters*, vol. 4, no. 2, pp. 438–443, Apr. 2020.
- [12] S. Calinon, F. D'halluin *et al.*, "Handling of multiple constraints and motion alternatives in a robot programming by demonstration framework," in *IEEE-RAS International Conference on Humanoid Robots*, Dec. 2009, pp. 582–588.
- [13] S. Calinon and A. Billard, "Statistical Learning by Imitation of Competing Constraints in Joint Space and Task Space," *Advanced Robotics*, vol. 23, no. 15, pp. 2059–2076, Jan. 2009.
- [14] S. Calinon, "A tutorial on task-parameterized movement learning and retrieval," *Intelligent Service Robotics*, vol. 9, no. 1, pp. 1–29, Jan. 2016.
- [15] A. Paraschos, R. Lioutikov *et al.*, "Probabilistic Prioritization of Movement Primitives," *IEEE Robotics and Automation Letters*, vol. 2, no. 4, pp. 2294–2301, Oct. 2017.
- [16] J. Silvério, S. Calinon *et al.*, "Learning Task Priorities from Demonstrations," *IEEE Transactions on Robotics*, vol. 35, no. 1, pp. 78–94, Feb. 2019.
- [17] D. Koert, G. Maeda *et al.*, "Demonstration based trajectory optimization for generalizable robot motions," in *IEEE-RAS International Conference on Humanoid Robots*, Nov. 2016, pp. 515–522.
- [18] A. Colomé and C. Torras, "Demonstration-free contextualized probabilistic movement primitives, further enhanced with obstacle avoidance," in *IEEE/RSJ International Conference on Intelligent Robots and Systems*, Sep. 2017, pp. 3190–3195.
- [19] D. Koert, J. Pajarinen *et al.*, "Learning Intention Aware Online Adaptation of Movement Primitives," *IEEE Robotics and Automation Letters*, vol. 4, no. 4, pp. 3719–3726, Oct. 2019.
- [20] A. Paraschos, C. Daniel *et al.*, "Using probabilistic movement primitives in robotics," *Autonomous Robots*, vol. 42, no. 3, pp. 529–551, Mar. 2018.
- [21] S. Gomez-Gonzalez, G. Neumann *et al.*, "Using probabilistic movement primitives for striking movements," in *IEEE-RAS International Conference on Humanoid Robots*, Nov. 2016, pp. 502–508.
- [22] —, "Adaptation and Robust Learning of Probabilistic Movement Primitives," *IEEE Transactions on Robotics*, vol. 36, no. 2, pp. 366–379, Apr. 2020.
- [23] R. Lioutikov, G. Neumann *et al.*, "Learning movement primitive libraries through probabilistic segmentation," *The International Journal of Robotics Research*, vol. 36, no. 8, pp. 879–894, Jul. 2017.
- [24] G. J. Maeda, G. Neumann *et al.*, "Probabilistic movement primitives for coordination of multiple human–robot collaborative tasks," *Autonomous Robots*, vol. 41, no. 3, pp. 593–612, Mar. 2017.
- [25] B. Siciliano and O. Khatib, *Springer Handbook of Robotics*. Springer, 2016.
- [26] T. Minka, "Divergence measures and message passing," Tech. Rep. MSR-TR-2005-173, Jan. 2005.
- [27] C. K. Williams and C. E. Rasmussen, *Gaussian Processes for Machine Learning*. MIT press Cambridge, MA, 2006.
- [28] G. S. Kimeldorf and G. Wahba, "A correspondence between Bayesian estimation on stochastic processes and smoothing by splines," *The Annals of Mathematical Statistics*, vol. 41, no. 2, pp. 495–502, 1970.
- [29] E. Wan and R. Van Der Merwe, "The unscented Kalman filter for nonlinear estimation," in *Proceedings of the IEEE 2000 Adaptive Systems for Signal Processing, Communications, and Control Symposium (Cat. No.00EX373)*, Oct. 2000, pp. 153–158.
- [30] M. Abadi, A. Agarwal *et al.*, "TensorFlow: Large-Scale Machine Learning on Heterogeneous Distributed Systems," p. 19.
- [31] D. P. Bertsekas, *Nonlinear Programming: Second Edition*. Athena Scientific, 2003.
- [32] J. Nocedal and S. J. Wright, *Numerical Optimization*, 2nd ed., ser. Springer Series in Operations Research. New York: Springer, 2006.
- [33] M. Charbonneau, F. Nori, and D. Pucci, "On-line joint limit avoidance for torque controlled robots by joint space parametrization," in *IEEE-RAS International Conference on Humanoid Robots*, Nov. 2016, pp. 899–904.
- [34] R. Lober, V. Padois, and O. Sigaud, "Multiple task optimization using dynamical movement primitives for whole-body reactive control," in *IEEE-RAS International Conference on Humanoid Robots*, Nov. 2014, pp. 193–198.
- [35] J. Silverio, S. Calinon *et al.*, "Bimanual Skill Learning with Pose and Joint Space Constraints," in *IEEE-RAS International Conference on Humanoid Robots*. Beijing, China: IEEE, Nov. 2018, pp. 153–159.



Felix Frank received his MSc degree in automation and control from RWTH Aachen University. He has worked as a research student in the field of optimal control for vehicle combustion engines. Felix joined the Volkswagen Group Machine Learning Research Lab in 2017 and he is currently pursuing a Ph.D. degree on topics related to stochastic optimal control and reinforcement learning in robotics.



Alexandros Paraschos received his Ph.D degree in computer science from Technical University of Darmstadt and is working in the areas of robotics and machine learning. During his PhD, he focused on Robot Learning for Complex Motor Skills. Before his PhD, Alexandros has been a research associate in Cognitive Robotics Research Centre (CRRC), at University of Wales. In 2017 he joined the Volkswagen Group Machine Learning Research Lab as a research scientist.



Patrick van der Smagt received his Ph.D. degree in mathematics and computer science from the University of Amsterdam. He is director of AI Research at Volkswagen Group, head of the Volkswagen Group Machine Learning Research Lab in Munich, and holds a honorary professorship at ELTE University Budapest. He previously directed a lab as professor for machine learning and biomimetic robotics at the Technical University of Munich while leading the machine learning group at the research institute fortiss. Patrick van der Smagt has won numerous awards, including the 2013 Helmholtz-Association Erwin Schroedinger Award, the 2014 King-Sun Fu Memorial Award, the 2013 Harvard Medical School/MGH Martin Research Prize, the 2018 Webit Best Implementation of AI Award, and best-paper awards at machine learning and robotics conferences and journals.



Botond Cseke received his Ph.D. degree in computer science from Radboud University Nijmegen. After post-doc positions at University of Edinburgh and Microsoft Research Cambridge, he joined the Volkswagen Group Machine Learning Research Lab in 2017 as a research scientist. He is interested in approximate probabilistic inference and related applications.